

ISTANBUL TECHNICAL UNIVERSITY ★ GRADUATE SCHOOL OF SCIENCE
ENGINEERING AND TECHNOLOGY

**EXPERIMENTAL INVESTIGATION OF FLOW STRUCTURES AROUND A
PLUNGING WING – FIXED TAIL COUPLE IN STEADY FLOW**

M.Sc. THESIS

**Ceyhun TOLA
(511101107)**

Department of Aerospace Engineering

Aerospace Engineering Programme

Thesis Advisor: Prof. Dr. M. Fevzi ÜNAL

Thesis Co-Supervisor: Assoc. Prof. Dr. N. L. Okşan ÇETİNER - YILDIRIM

JANUARY 2012

İSTANBUL TEKNİK ÜNİVERSİTESİ ★ FEN BİLİMLERİ ENSTİTÜSÜ

**SERBEST AKIMA DİK DOĞRULTUDA SALINIM YAPAN KANAT - SABİT
KUYRUK ÇİFTİNİN ETRAFINDAKİ AKIM YAPISININ DENEYSEL
OLARAK İNCELENMESİ**

YÜKSEK LİSANS TEZİ

**Ceyhun TOLA
(511101107)**

Uçak ve Uzay Mühendisliği Anabilim Dalı

Uçak ve Uzay Mühendisliği Programı

Tez Danışmanı: Prof. Dr. M. Fevzi ÜNAL

Eş Danışman: Doç Dr. N. L. Okşan ÇETİNER - YILDIRIM

OCAK 2012

Ceyhun Tola, a **M.Sc.** student of ITU **Institute of / Graduate School of Science Engineering and Technology** student ID **511101107**, successfully defended the **thesis/dissertation** entitled “**EXPERIMENTAL INVESTIGATION OF FLOW STRUCTURES AROUND A PLUNGING WING – FIXED TAIL COUPLE IN STEADY FLOW**”, which he prepared after fulfilling the requirements specified in the associated legislations, before the jury whose signatures are below.

Thesis Advisor : **Prof. Dr. M. Fevzi Ünal**
İstanbul Technical University

Co-advisor : **Assoc. Prof.Dr. N. L. Okşan ÇETİNER**
YILDIRIM
İstanbul Technical University

Jury Members : **Prof. Dr. Fırat Oğuz EDİS**
İstanbul Technical University

Prof. Dr. Erkan AYDER
İstanbul Technical University

Prof. Dr. Kadir KIRKKÖPRÜ
İstanbul Technical University

Date of Submission : 16 December 2011

Date of Defense : 19 January 2012

To my mother,

FOREWORD

Accomplishing an experimental M.Sc. education in a short time is only substantiated with strong support and guidance with considerably experienced advisors. Therefore, I would like to thank endlessly to my supervisor Prof. Dr. M. Fevzi Ünal and to my co-supervisor Assoc. Prof. Dr. N. L. Okşan Çetiner – Yıldırım for their guidance and support.

I would like to thank my idol Prof. Dr. A. Rüstem Aslan since he not only encouraged me for interdisciplinary working, but also I felt his support behind my every step and every work throughout my M.Sc. life. His support and confidence was inestimable.

I would also like to express my gratefulness to my dearest friend Serdar Seçkin. His physical and spiritual support during the experiments was incredible. I will always remind his friendship and kindness.

I would like to extend my thanks to the staff of Trisonic Laboratory and my dear fellow workers: Onur Son, S. Banu Yılmaz, Ali Eken for their friendship, endless support and eagerness to help whenever I encountered a problem.

Then I would like to thank to all my friends for their friendship and support.

Additionally, I would like to thank endlessly to all other nameless heroes: founders and supporters of the Trisonic Laboratory. I owe this work to their valuable struggle.

Finally, I would like to express my gratitude to my dear mother. She has always been a source of pride and inspiration for me. Her endless confidence and support helped me accomplish this work in time. I am indebted to her.

December 2011

Ceyhun TOLA
Aeronautical &
Astronautical
Engineer

TABLE OF CONTENTS

	<u>Page</u>
FOREWORD	ix
TABLE OF CONTENTS	xi
ABBREVIATIONS	xiii
LIST OF TABLES	xv
LIST OF FIGURES	xvii
LIST OF SYMBOLS	xix
SUMMARY	xxi
ÖZET	xxiii
1. INTRODUCTION	1
1.1 General Information About Flapping Wings	1
1.2 Purpose of the Thesis	3
1.3 General Parameters and Geometry of 2D Plunging Motion and Applications ..	3
1.4 Literature Review	7
2. EXPERIMENTAL SETUP AND DATA ACQUISITION	25
2.1 Flow System	25
2.2 Experimental Models and Montage	27
2.3 Airfoil Motion	30
2.4 Digital Particle Image Velocimetry Method	31
2.4.1 Seeding	32
2.4.2 Data Recording	33
2.4.3 Illumination	34
2.4.4 Synchronization	35
2.4.5 Correlation	35
2.4.6 Masking, Validation and Other Processes	36
2.5 Experiments.....	36
2.5.1 Image Acquisition	36
2.5.2 Post Processing	38
3. RESULTS	43
3.1 Effects of Doubling the Plunging Frequency and Reynolds Number	45
3.2 Investigation of the Best Tail Position and Orientation for Drag Minimization and Thrust Maximization	48
3.3 Effects of Changing the Tail Airfoil with a Flat Plate	64
4. CONCLUSION	67
5. REFERENCES	69
APPENDICES	75
APPENDIX A.1	76
CURRICULUM VITAE	79

ABBREVIATIONS

AOA_{max}	: Maximum Angle of Attack
CCD	: Charged Couple Device
CFD	: Computational Fluid Dynamics
CNC	: Computer Numerical Control
DPIV	: Digital Particle Image Velocimetry
LDA	: Laser Doppler Anemometry
LEV	: Leading Edge Vortex
LDV	: Laser Doppler Velocimetry
MAV	: Micro Air Vehicle
PIV	: Particle Image Velocimetry
POD	: Proper Orthogonal Decomposition
RANS	: Reynolds Averaged Navier-Stokes Solver
RPM	: Revolution per Minute
SEREP	: System Equivalent Reduction Expansion Process

LIST OF TABLES

	<u>Page</u>
Table 2.1 : Basic Specifications of Kollmorgen/Danaher Servo Motor.	31
Table 2.2 : Seeding Materials for Liquid Flows (Cetiner, 2010)..	33
Table 2.3 : Image Properties After the Stitching Process.	40
Table 3.1 : Summary of the Experimental Parameters.....	43
Table 3.2 : Data Acquisition Parameters.....	44
Table 3.3 : Effects of Doubling the Reynolds Number and the Plunging Frequency for $d=5$ and $\alpha=30^\circ$	46
Table 3.4 : Effects of Doubling the Reynolds Number and the Plunging Frequency for $d=0$ and $\alpha=0^\circ$	47
Table 3.5 : Instantaneous Vorticity Patterns for Different Tail Positions and Orientations-1.....	49
Table 3.6 : Instantaneous Vorticity Patterns for Different Tail Positions and Orientations-2.....	50
Table 3.7 : Instantaneous Vorticity Patterns for Different Tail Positions and Orientations-3.....	51
Table 3.8 : Instantaneous Vorticity Patterns for Different Tail Positions and Orientations-4.....	52
Table 3.9 : Instantaneous Vorticity Patterns for Different Tail Positions and Orientations-5.....	53
Table 3.10 : Instantaneous Vorticity Patterns for Different Tail Positions and Orientations-6.....	54
Table 3.11 : Averaged Velocity Profiles ($U-U_\infty$) for Different Tail Positions and Orientations-1.....	56
Table 3.12 : Averaged Velocity Profiles ($U-U_\infty$) for Different Tail Positions and Orientations-2.....	57
Table 3.13 : Averaged Velocity Profiles ($U-U_\infty$) for Different Tail Positions and Orientations-3.....	58
Table 3.14 : Averaged Resultant Velocity Profiles (U) for Different Tail Positions and Orientations-1.	59
Table 3.15 : Averaged Resultant Velocity Profiles (U) for Different Tail Positions and Orientations-2.	60
Table 3.16 : Averaged Resultant Velocity Profiles (U) for Different Tail Positions and Orientations-3.	61
Table 3.17 : Effects of Replacing the Tail Airfoil with a Flat Plate for $Re=10000$ and $d=0$	65
Table 3.18 : Effects of Replacing the Tail Airfoil with a Flat Plate for $Re=10000$ and $d=5$ cm.....	66
Table A.1 : List of the Experiments	76
Table A.2 : Meaning of the Camera Numbers	78

LIST OF FIGURES

	<u>Page</u>
Figure 1.1 : Flapping Wing Designs from Past to Present.....	2
Figure 1.2 : Settlements of the Plunging Wing and the Tail for different d and α values.....	3
Figure 1.3 : Plunging Motion (adopted from Percin, 2009)..	4
Figure 1.4 : General Aerodynamic Knowledge Database in terms of Reduced Frequency and Reynolds number (adopted from Ames et al. 2001)..	6
Figure 1.5 : Strouhal Numbers of Different Species of Fliers and Swimmers (adopted from Taylor et al., 2003)..	6
Figure 1.6 : Illustration on Knoller – Betz Effect (adopted from Platzer et al., 2008)..	7
Figure 1.7 : Illustration of Karman and Reverse Karman Streets (adopted from Jones et al., 1998).	8
Figure 1.8 : Different Wake Configurations Depending on the Plunging Velocity (kh) (adapted from Jones et al., 1998)..	9
Figure 1.9 : Drag/Thrust as a Function of h and k (adopted from Jones et al., 1996)..	10
Figure 1.10 : Transition from Normal to Reverse Karman Vortex Street with Increasing kh (adopted from Lai and Platzer, 1999)..	10
Figure 1.11 : Wake Configurations as a Function of Reduced Frequency (k) and Non-dimensional Plunge Amplitude (h) (adopted from Percin, 2009)..	14
Figure 1.12 : Large Scale Water Channel	22
Figure 2.1 : Summary of the Experimental Parameters	25
Figure 2.2 : External Filters and Centrifugal Pump	26
Figure 2.3 : Controller of the Centrifugal Pump.....	26
Figure 2.4 : Images of Wing, Tail and Flat Plate.....	28
Figure 2.5 : Images of the Ruler for Flat Plate and C Shaped Support.....	28
Figure 2.6 : Images of the Rulers for Tail Montage.....	29
Figure 2.7 : Mountage of one of the Experimental Cases.....	29
Figure 2.8 : Grid.....	30
Figure 2.9 : Labview VI.....	30
Figure 2.10 : Kollmorgen/Danaher Motion AKM33E Servo Motor and Its Gear System	31
Figure 2.11 : Summary of DPIV’s Basic Principle (Url-1)	32
Figure 2.12 : Silver Coted Hollow Glass Particles.	33
Figure 2.13 : Flow Sense Cameras.....	34
Figure 2.14 : Dual Cavity Nd:Yag Laser	34
Figure 2.15 : Synchronization of the System (Andersen, 2007)..	35
Figure 2.16 : Double Frame / Single Exposure Recordings, The Digital Cross Correlation Method (adopted from Raffel et al, 1998).....	35

Figure 2.17 : Experimental Arrangement for Two Different Camera Locations.....	37
Figure 2.18 : Sample DPIV Image Before and After the Stitching Process.	39
Figure 2.19 : Field of View of the Cameras for Two Different Positions.	40
Figure 2.20 : Vector Cleaning Process.....	41
Figure 3.1 : Sinusoidal Motion of the Plunging Airfoil.	44
Figure 3.2 : Variation of Thrust/Drag Production Depending on Position and Orientation of the Tail for $h=0.25$ and $f=0.2$ Hz	62
Figure 3.3 : Variation of Thrust/Drag Production Depending on Position and Orientation of the Tail for $h=0.05$ and $f=0.4$ Hz.	63
Figure 3.4 : Variation of Thrust/Drag Production Depending on Position and Orientation of the Tail for All Cases.....	64

LIST OF SYMBOLS

A	: Wake width
c	: Airfoil chord
c_l	: Airfoil lift coefficient
d	: Distance between trailing edge of plunging airfoil and leading edge of tail airfoil
f	: Plunging frequency
h	: Non-dimensional plunge amplitude
Re	: Reynolds number
k	: Reduced frequency
St	: Strouhal number
T	: Period of plunge motion
U_∞	: Free stream velocity
α	: Tail's angle of attack
α_{eff}	: Effective angle of attack of the airfoil
μ	: Dynamic viscosity
ρ	: Density
ϕ	: Phase angle

EXPERIMENTAL INVESTIGATION OF FLOW STRUCTURES AROUND A PLUNGING WING – FIXED TAIL COUPLE IN STEADY FLOW

SUMMARY

Humans have always observed and tried to mimic the nature for meeting their needs. Since transportation was a critical necessity for them, they searched ways of flight by observing low Reynolds number fliers like birds and insects. Therefore, they focused on developing flapping wing systems up to 1900s. At the beginning of the 20th century, researchers recognized that it was also possible to fly with fixed wing systems; furthermore, design and manufacturing of these systems were easier than design and manufacturing of the flapping wing systems. Thus, the general interest on flapping wing design was not appreciable up to 1980s. However, it is impossible to accomplish some kind of missions with fixed wing air vehicles. For instance, fixed wing vehicles cannot fly at low Reynolds numbers while flapping wing designs can. Therefore, towards the end of the 20th century flapping wing air vehicle design has become popular with an increased demand.

Today, many researchers have been conducting projects about Micro Air Vehicle (MAV) design. MAVs are small unmanned air vehicles that can be used for risky military or commercial missions and for other useful jobs like traffic monitoring etc. While designing a MAV, it is crucial to develop an efficient vehicle. Therefore researchers have to select the flapping parameters carefully. Additionally, the location of wing and tail has to be determined since it affects the performance of the vehicle too since it may be possible to reduce or increase thrust – drag force produced by flapping wing. Therefore, in this study, the possibility of decreasing drag or increasing thrust production using vortical interactions arising from placement of a tail airfoil behind a plunging wing is investigated by Digital Particle Image Velocimetry (DPIV) Method for making a contribution to the development of new generation of more efficient Micro Air Vehicles. Additionally, the effect of doubling the plunging frequency and the Reynolds number on flow structure is also examined within the scope of this work. As a final effort, the effect of replacement of the tail airfoil with a flat plate having same length on flow structure (only for 0 deg angle of attack) is investigated.

Experiments are conducted in a Large Scale Water Channel located at the Trisonic Research Laboratory of Istanbul Technical University. Oscillation of the airfoil is provided by a servo motor controlled by 2 different computers. All experimental data are gathered via 2 CCD cameras by illumination of the examined flow plane with a Nd: Yag Laser. Gathered data is stored on a data acquisition computer and processed via a sequence of programs. Data post processing steps consists of image stitching, cross correlation, determination of the objects' coordinates on the image and masking of them, elimination of bad vectors, assignment of average vectors for

deleted ones, and finally calculation of the average value of the vectors using all images' vector maps. Then, results are examined using Tecplot program.

Experimental results showed that, reducing the distance between the tail airfoil and the plunging wing starts to change the direction of vortices shedding from oscillating wing by crossing their paths and this causes the alteration of the amount thrust or drag. No thrust production but drag reduction is observed when the tail airfoil is close enough to the plunging wing for all experimental cases and any increment in tail airfoil's angle of attack is also resulted in the increment of the total drag force as expected. Additionally, experiments revealed that the flow structure does not change with doubling both Reynolds number and plunging frequency; instead, it strengthens existing vortex structure. The flow structure exhibited almost the same behavior when the tail airfoil is replaced with a thin flat plate having the same chord length (for 0 degree tail angle).

SERBEST AKIMA DİK DOĞRULTUDA SALINIM YAPAN KANAT – SABİT KUYRUK ÇİFTİNİN ETRAFINDAKİ AKIM YAPISININ DENEYSEL OLARAK İNCELENMESİ

ÖZET

Leonardo Da Vinci'den başlayarak 1900'lü yılların başlarına kadar kanat çırparak uçan araçlar geliştirmeye çalışan insanoğlu, 1900'lü yılların başlarında sabit kanatlı hava araçlarının tasarım ve üretim kolaylığının farkına varmış ve sabit kanatlı araçlar geliştirilmeye koyulmuştur. Bu süreçte, çırpın kanatlı hava araçlarına olan ilgi ve tasarım için harcanan zaman azalmış; böylelikle sabit kanatlı hava araçları ön plana çıkmıştır. Süreç ilerledikçe, talep edilen ihtiyacı karşılayacak birçok sabit kanatlı hava aracı üretilmiştir. 20. yüzyılın sonlarına doğru çeşitli görevlerde kullanılmak üzere oldukça düşük seyir hızlarında uçabilen, mümkün olduğunca küçük hava araçlarının üretilmesi talep edilmiş ve böylelikle çırpın kanatlı hava aracı tasarımı ve üretiminin önü açılmıştır.

Kanat çırparak uçan hava araçlarının en büyük avantajı düşük seyir hızlarında tutunma kaybı yaşamadan havada tutunabilmeleridir. Üstelik bu tür araçlar döner kanatlı hava araçlarına göre çok daha az gürültü üretmekte ve enerji tüketmektedir. Teknolojinin hızlı ilerleyişiyle birlikte boyutları 15 cm'den daha küçük olan hava araçlarının üretimine başlanmıştır. Bu araçlara kısaca Mikro Hava Araçları (MHA) adı verilmektedir. Mikro Hava Araçları, fiziksel olarak ulaşılması mümkün olmayan tehlikeli ya da insan sağlığı açısından risk teşkil eden bölgelerden veri toplanması vb. görevleri rahatlıkla yerine getirebilirler. Ayrıca gözlem, haritalama gibi birçok sivil ve askeri görevde kullanılabilirler.

Çırpın kanatlı mikro hava araçlarının tasarımında en önemli kıstaslardan birisi araçların verimidir. Aracın verimi, onun tüketeceği enerji ve havada kalış süresini dolaylı olarak etkilemektedir. İyi bir aracın mümkün olduğunca az enerjiyle, olabilecek en uzun süre havada kalması ya da mümkün olan en uzun mesafeyi kat etmesi istenir. Bunu sağlayabilmek için boyutlandırmalar özenle yapılarak, kanat çırpma parametreleri dikkatlice seçilmelidir. Bu sayede hava aracının üreteceği itkiyi artırmak mümkündür.

Bir kuş gibi kanat çırpma oldukça zordur. Hareketin karmaşık olması ve birçok hareketin birleşiminden oluşması nedeniyle kanat çırpma hareketi değişik alt hareketlerin ayrı ayrı incelenmesiyle ele alınabilir. Genellikle yunuslama, akıma dik doğrultuda salınım yapma ve bu iki hareketin bileşimi incelenmektedir. Bu çalışmada sadece akıma dik doğrultuda salınım yapan bir kanat kullanılmıştır.

İki önemli çırpın kanat parametresi bulunmaktadır. Bunlar: a) İndirgenmiş frekans (k) ve b) Boyutsuz genlik (h)' tir. İndirgenmiş frekans kanat çırpma frekansıyla, boyutsuz genlik ise kanat çırpma genliği ile doğru orantılıdır. Bu iki değer in çarpılmasıyla oluşan kh değeri bize kanadın belirli şartlar altında itki mi sürüklemeye mi ürettiğini bildirmesi bakımından oldukça önemlidir.

Doğru kanat çırpma parametrelerini belirleyebilmek adına bugüne kadar birçok araştırma gerçekleştirilmiştir. Belirli bir kanadın itki mi sürüklenme mi ürettiği iz bölgesine bakılarak anlaşılabilir. Kabaca, eğer kanadın iz bölgesinde bir momentum artışı varsa, kanat itki; momentum kaybı mevcutsa, kanat sürüklenme ürettiği demektir. Yürütülen araştırmalar ve gerçekleştirilen deneyler sonucunda yukarıda bahsedilen kh çarpım değerinin 0,4'ten küçük olması durumunda kanadın sürüklenme, bu değerden büyük olması durumunda ise itki ürettiği anlaşılmıştır. Aslında bu durum, çırpma kanadın arkasında oluşan girdap yapısının, kanat çırpma parametrelerine bağlı değişiminden kaynaklanmaktadır. Kanat arkasından kopan girdapların bir jet akışı oluşturacak şekilde bir araya gelmesi itki üretimine yol açar, aksi ise momentum kaybının ortaya çıkmasına yani sürüklenme oluşmasına neden olur.

Bu çalışmanın esas amacı, çırpma kanat arkasına yerleştirilen bir kuyruğun kanat arkasındaki girdaplarla etkileşime girerek, kanadın üretmekte olduğu sürüklemeyi itkiye çevirip çeviremeyeceğini ya da mevcut sürüklemeyi azaltıp azaltamayacağını araştırmaktır. Ayrıca çalışma kapsamında kanat çırpma frekansı ve Reynolds sayısı iki katına çıkarılarak bunun akış yapısını ne şekilde değiştirdiği araştırılmıştır. Son olarak, çırpma kanadın arkasına yerleştirilen kanat profili geometrisine sahip çırpma kanadın yarı veter uzunluğuna sahip kuyruk aynı uzunluktaki 1,5 mm kalınlığa sahip ince bir levhayla değiştirilmiş ve bu değişimin akış yapısını nasıl etkilediği incelenmiştir (sadece 0 derece kuyruk hücum açısı için bu inceleme yapılmıştır).

Akış alanı Sayısal Parçacık Görüntülenmesi ile Hız Ölçümü (DPIV) yöntemiyle görüntülenmiştir. Deneyler, Trisonik Araştırma Laboratuvarındaki 710 mm x 1010 mm kesitinde test bölgesine sahip 14 ton su kapasiteli su kanalında gerçekleştirilmiştir. Ölçümler 2 farklı kamera konumu kullanılarak alınmış böylelikle hem akış alanı hem de yakın iz bölgesi görüntülenmiştir.

Veri alınması işleminde 3 farklı bilgisayar görev yapmıştır. Bu bilgisayarlardan bir tanesi veri alım ve depolama işlemlerini, diğer ikisi de servo motorun kontrolünü sağlamıştır. Sistemde görev yapan zamanlayıcı, lazerin çakma ve kameraların veri alma senkronizasyonunu sağlamaktadır.

Çalışma kapsamında, çırpma kanadın kendi başına itki ve sürüklenme ürettiği 2 farklı kh değeri için ölçümler alınmıştır. Her bir kh değerinde çırpma kanadın arkasına 4 farklı mesafede ve 3 farklı açıda kuyruk yerleştirilerek, kuyruk-kanat sisteminin etkisinin ve sürüklenmesinin yalnız başına akıma dik doğrultuda salınım yapan kanada göre nasıl değiştiği incelenmiştir. Ayrıca kanat çırpma frekansı ve serbest akış hızı iki katına çıkarılarak akış yapısındaki değişim gözlenmiştir. Son olarak, 0 derece kuyruk hücum açısında kanat profili yerine düz levha kullanmanın nasıl bir fark yaratacağı, 0 derecede kuyrukla yapılan deneylerin düz levhayla tekrarlanması sağlanarak araştırılmıştır.

Deneylerin tamamlanması ve verilerin bilgisayarda depolanmasının ardından farklı kameralardan alınan veriler bir MATLAB kodu yardımıyla yapılandırılmış, daha sonra birleştirilmiş her bir fotoğraf için vektör alanı edilmiştir. Çırpma kanadın ve kuyruğun yerini hesaplayarak her fotoğraf için bu cisimleri maskeleyen programlar kullanılmış, böylelikle hatalı sonuçlar alınması engellenmiştir. Maske alanındaki vektörlerin filtrelenmesinin ardından fotoğrafta bulunan ve ışık azlığı vb. sebeplerle ortaya çıkan hatalı vektörler CleanVec isimli bir program tarafından ayıklanmıştır. Daha sonra ayıklanan vektörlerin yerine bir başka program tarafından ortalama vektörler tanımlanmıştır.

Her bir deney seti için 10 Hz frekansta çekim yapılarak 200 adet fotoğraf alınmıştır. Veri işleme aşamasının sonunda bu 200 fotoğraftaki işlenmiş vektör alanlarının ortalamaları NWENSAW isimli bir program tarafından hesaplanmış ve böylelikle çırpan kanat-kuyruk sisteminin üretmiş olduğu itki sürüklenme durumları incelenmiştir.

Yapılan deneyler sonucunda, çırpan kanadın yalnız başına sürüklenme ürettiği kh değerinde, arkasına farklı mesafelerde yerleştirilen kuyruk, kanada yaklaştıkça, kanattan kopan girdaplarla etkileşime girmiş ve onların yolunu kesmiştir. Kuyruk ile kanat arasındaki mesafe 2.5 cm den 0 cm e kadar azaltıldığında (yani kuyruk kanada teğet konuma getirildiğinde) bu etkileşim en üst seviyeye ulaşarak üretilen sürüklemeyi azaltmıştır. Ancak mevcut sürüklemeyi itkiye dönüştürememiştir. Çırpan kanadın yalnız başına itki ürettiği kh değerinde, arkasına farklı mesafelerde yerleştirilen kuyruk, sistemin sürüklenme üretmesine yol açmıştır, önceki deney setlerinde olduğu gibi burada da kuyruk kanada yaklaştıkça, kanattan kopan girdaplarla etkileşime girmiştir. Kuyruk kanada teğet duruma getirildiğinde sistemin ürettiği sürüklenme de girdap etkileşimleri nedeniyle azalmıştır. Ayrıca tüm deney setlerinde, kuyruk hücum açısının artırılması beklenildiği üzere üretilen sürüklemenin artmasına yol açmıştır.

Kanat çırpma frekansı ve serbest akım hızının (dolayısıyla Reynolds sayısının) iki katına çıkarılması sadece aynı akış yapısına ve daha kuvvetli girdaplara sahip bir akış yapısı oluşmasına yol açmıştır. Diğer bir deyişle, bu parametreleri iki katına çıkarmak girdapların yerinde bir değişime yol açmamış, sadece onları şiddetlendirmiştir.

Son olarak, 0 derece hücum açısı için gerçekleştirilen deneylerde, kanat geometrisine sahip kuyruğun, aynı veter uzunluğuna sahip ince, düz bir levhayla değiştirilmesi, önceki ile neredeyse aynı akış yapısının oluşmasına yol açmıştır. Akış yapısında meydana gelen ihmal edilebilir derecede küçük değişiklikler, kanat geometrisine sahip kuyruğun sivri firar kenarına ve yumuşak bir hücum kenarına sahip olmasından kaynaklanmaktadır.

Çalışma kapsamında elde edilen veriler yeni nesil mikro hava araçlarının kuyruk konumunun ve açısının belirlenmesinde yardımcı olacaktır.

1. INTRODUCTION

1.1 General Information About Flapping Wings

Mankind has always been inspired from the nature for meeting their needs and finding new solutions to their problems. Since transportation is one of the biggest necessity for humans, they sought out alternative ways to access from one place to another as fast as possible and thus, they observed the natural fliers like birds, bats and insects etc. Trying to imitate birds' wings many people struggled to fly and they tried to design various systems resembling birds' wings. Leonardo Da Vinci, the most famous designer in the 15th century, working on not only the flight of the birds but also their wings' structure, he designed and drew the detailed plans of different types of flight machines like human-powered ornithopter and mechanical wing devices. Since his designs were far beyond his time, the fascinating flight machines could not be tested in those years.

At the beginning of the 20th century, with recognition of the fixed wing design's ease of manufacture, engineers designed and produced fixed wing flight machines and this innovation decreased the general interest on flapping wing design up to 1980s. Although, fixed wing air vehicles' design and production is much easier than the flapping wing air vehicle design, there are lots of duties in which the fixed wing air vehicles cannot be used due to their large dimensions and owing to the obligations that they have to fly at relatively high Reynolds numbers. In order to design special air vehicles having capability of flying at low speeds efficiently, scientists have been interested in the basic mechanisms of animal locomotion again.

Studies about flapping wings have a big importance today since they have a great role on development of Micro Air Vehicles (MAVs) which are a special class of unmanned air vehicles having dimensions not more than 15 centimeters. MAVs have been designing for both military and commercial missions. Their hovering and high maneuverability capabilities enable them to be used in hazardous areas which cannot be accessible via ground vehicles and they are also suitable for reconnaissance and

surveillance missions. Additionally, they can also be used for traffic monitoring applications. Since MAVs are designed to spend only a little power in flight and they can recharge their batteries with natural sources like sun, wind and even the vibration of a wire, they will probably maintain their mission during days without giving any break in future.

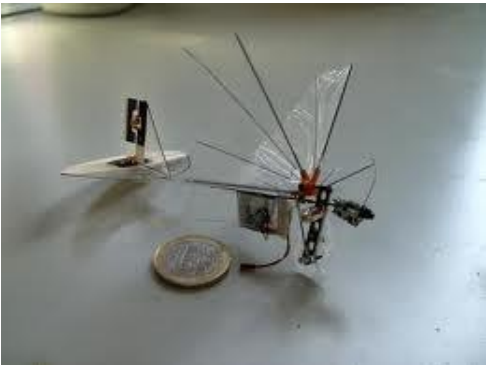
Micro Air Vehicles should be aerodynamically efficient in low Reynolds number regime in order to use them in building interiors or closed complex structures. Therefore scientists have been working on understanding the propulsive mechanism of low Reynolds number fliers and conducting studies for perceiving the physics of unsteady flow structure interaction problems to design an efficient MAV. Since there are lots of parameters affecting the MAVs' performance and power consumption; and there is also a rapidly increasing demand for MAV development; the number of scientists and researchers interested in flapping wing air vehicle design is increased rapidly.



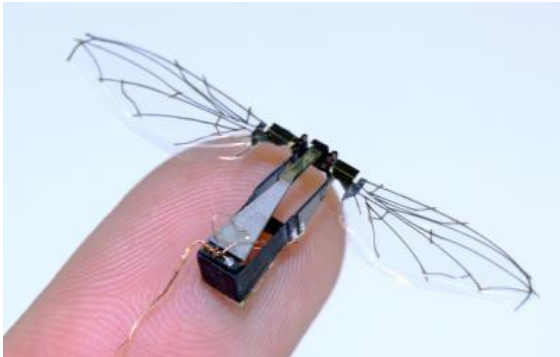
Leonarda Da Vinci's Flapping Wing (1489)



Leonarda Da Vinci's Ornithopter (1490)



Delfly Micro Air Vehicle (2006)



Harvard Microbotic Fly (2010)

Figure 1.1 : Flapping Wing Designs from Past to Present.

1.2 Purpose of the Thesis

The aim of this study is to determine the effects of tail's location and its angle of attack on plunging two-dimensional NACA0012 airfoil's thrust/drag production in a steady flow by observing the vortex interactions and analyzing the wake region of the airfoils. The effects of horizontal distance between the airfoil and the tail and the effects of tail's angle of attack on vortex structure behind them are investigated experimentally via Digital Particle Image Velocimetry (DPIV) in a large scale water channel.



Figure 1.2 : Plunging Wing and the Tail for different d and α values.

After this study the appropriate tail location and tail angle for a plunging Micro Air Vehicle can be predicted and results of the experiments will probably be used for designing more efficient MAVs.

1.3 General Parameters and Geometry of 2D Plunging Motion and Applications

Plunging motion can be modeled with a $y(t)$ function. In this study, NACA 0012 airfoil is plunged sinusoidally. Therefore the $y(t)$ function representing the sinusoidally plunging airfoil's motion can be written as follows:

$$y(t) = y_0 + a \cdot \sin(2\pi ft + \phi) \quad (1.1)$$

In Equation (1.1), y_0 represents the initial position of the plunging airfoil, a can be named as plunge amplitude, f stands for the plunge frequency and ϕ is defined as the phase angle of the plunging motion.

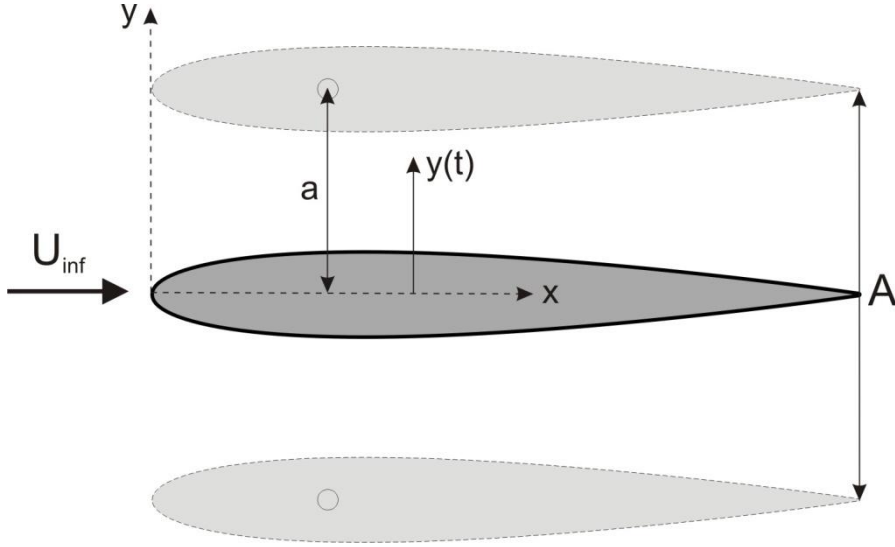


Figure 1.3 : Plunging Motion (adopted from Percin, 2009).

Illustration of the plunging airfoil's motion can be seen in Figure 1.3.

The plunge motion's behavior is characterized by two significant non-dimensional parameters which are reduced frequency symbolized with k and non-dimensional plunge amplitude symbolized with h .

Non-dimensional plunge amplitude (h) is the dimensionless version of plunge amplitude (a). Therefore it can be written as follows:

$$h = \frac{a}{c} \quad (1.2)$$

The reduced frequency (k) is the dimensionalized version of the plunge frequency (f) using the chord length of the airfoil (c) and the free-stream velocity (U_∞). The formulation used in this study can be seen from Equation (1.3).

$$k = \frac{\pi f c}{U_\infty} \quad (1.3)$$

However, in some studies the reduced frequency is defined as Equation (1.4):

$$k = \frac{2\pi f c}{U_\infty} \quad (1.4)$$

Therefore while making comparisons of the results with different studies, this critical point have to be considered.

Strouhal number symbolized with St is another important parameter generally used in the flapping wing studies.

$$St = \frac{fA}{U_\infty} \quad (1.5)$$

where A (wake width) is the distance equal to $2a$ (for 2D plunging motion) which is illustrated in Figure 1.3. Therefore, it can be written as in Equation (1.6).

$$St = \frac{2fa}{U_\infty} = \frac{2\pi fc a}{U_\infty c \pi} = \frac{kh}{\pi} \quad (1.6)$$

Another widely used parameter in fluid mechanics: Reynolds number symbolized with Re is defined as the ratio of inertial forces to viscous forces. In this study, formulation of the Reynolds number can be written as follows:

$$Re = \frac{\rho U_\infty c}{\mu} \quad (1.7)$$

where ρ is the density and μ is the dynamic viscosity of the fluid of the fluid.

Plunging motion of an airfoil in a uniform flow leads to resultant velocity vector which is at an angle with the chord line. This angle is called as the effective angle of attack symbolized with α_{eff} . Formulation of it can be seen from Equation (1.8).

$$\begin{aligned} \alpha_{eff} &= \tan^{-1} \frac{y}{U_\infty} = \tan^{-1} \frac{a}{c} \frac{2\pi fc}{U_\infty} \cos(2\pi ft + \phi) \\ &= \tan^{-1} 2kh \cdot \cos(2\pi ft + \phi) \end{aligned} \quad (1.8)$$

After defining these critical parameters, in order to have an opinion about their values and usages following figures are given.

From the Figure 1.4 it can be stated that higher reduced frequency levels enables small insects to fly at low Reynolds numbers.

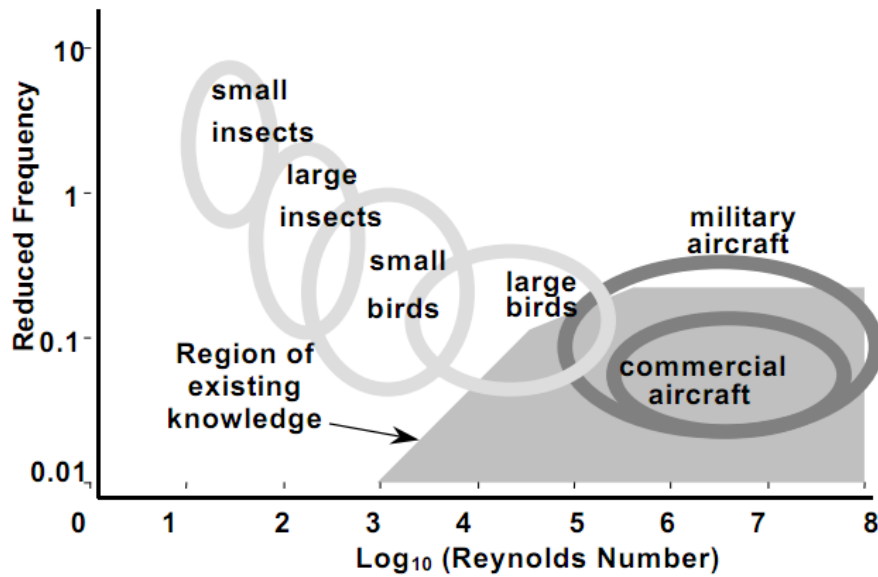


Figure 1.4 : General Aerodynamic Knowledge Database in terms of Reduced Frequency and Reynolds number (adopted from Ames et al. 2001).

Figure 1.5 represents the values of Strouhal numbers belonging to different species of birds', bats' and insects' cruising flight data.

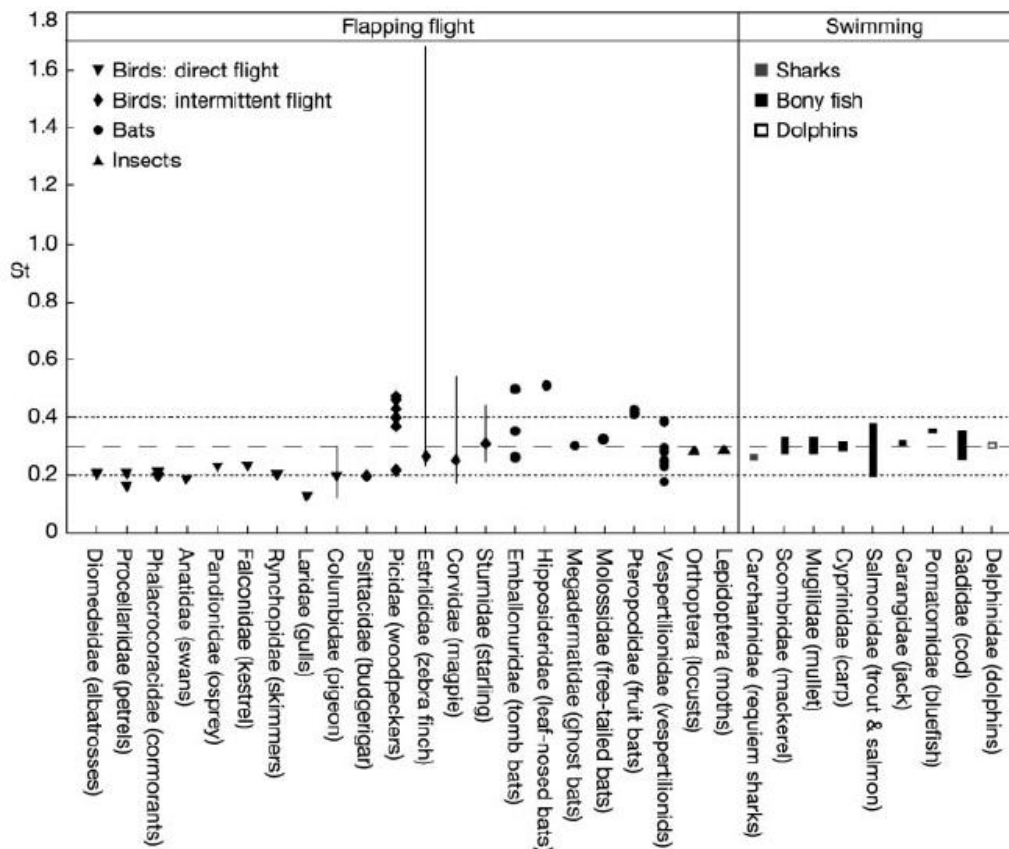


Figure 1.5 : Strouhal Numbers of Different Species of Fliers and Swimmers (adopted from Taylor et al., 2003).

1.4 Literature Review

Flying with a flapping wing is a dream for mankind since Leonardo Da Vinci and several flapping wing studies have been conducted by both scientists and engineers. While some of the studies investigate the flow around flapping wings using numerical methods in order to guide the experiments, experimental methods are also used for investigating the nature of the flapping wings to verify the numerical results and for revealing the flow field exactly. The contents of studies can be classified according to flapping wing's motion whether they include plunging, pitching or both of them. Additionally, studies investigating the effects of different objects' motions on the flow field (interacting with each other) can also be considered as another class.

The two important pioneers of the flapping wing studies: Knoller (1909) and Betz (1912) revealed that plunging wings generate a lift force having thrust component in the direction of free stream velocity (Knoller – Betz Effect) and this effect was verified experimentally by Katzmayr in 1922. According to them the lift and thrust is a product of an effective angle of attack arising from the harmonically plunging motion (Figure 1.6).

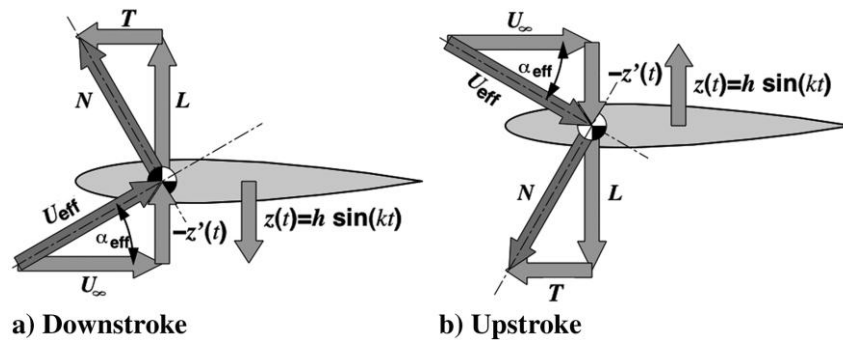


Figure 1.6 : Illustration on Knoller – Betz Effect (adopted from Platzer et al., 2008).

Jones, Dohring and Platzer (1998) investigated the Knoller-Betz Effect both experimentally and numerically. They visualized the wake formations of plunging airfoils using Laser Doppler Velocimetry (LDV) in a close circulating water channel to determine the effect of plunge frequency and amplitude on the wake characteristic. Experimental results are compared with numerical computations using previously developed inviscid, unsteady panel code utilizing a non-linear wake model. Comparisons showed that experimental and numerical results are well matched over

a broad range of reduced frequencies and Strouhal numbers. Therefore, they stated that formation and development of thrust-indicative wake structures are primarily inviscid phenomena. According to their study, at very low Strouhal numbers drag is generated due to viscous effects.

Von Karman and Burgers (1943) stated that drag and thrust production is a result of location and orientation of the wake vortices. According to Jones, et al. (1998) the thrust or drag generation of the system can be determined analyzing the wake of the system. If the wake of the system seemed to be a Karman Vortex Street as seen in Figure 1.7-a then it can be said that system produces drag since there is a momentum deficit. If the wake of the system seemed to be a Reverse Karman Vortex Street as seen in Figure 1.7-b then it can be said that system produces thrust since there is a jet like flow.

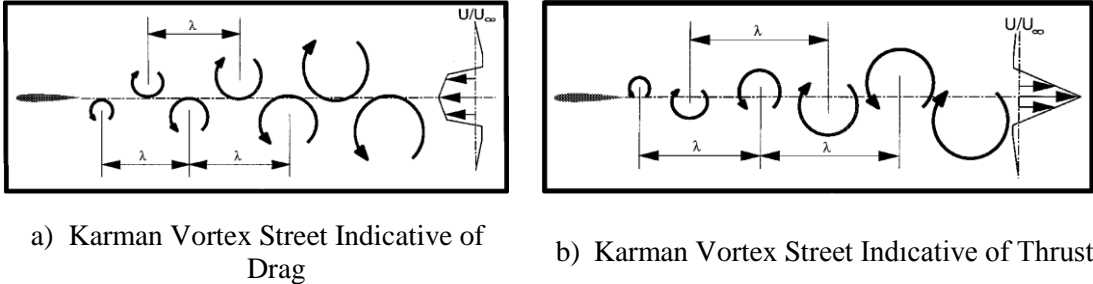


Figure 1.7 : Illustration of Karman and Reverse Karman Streets (adopted from Jones et al., 1998).

The vertical distance between the upper and the lower vortex row has a special significance on the amount of momentum deficit or superfluity. According to Young (2005) if this distance close up and goes to zero, no force is generated which is known as the neutral wake structure seen in Figure 1.8-b.

According to Jones, Dohring and Platzner (1996) different wake formations occurs after the plunging airfoil as a result of the increment of the plunge velocity which is the product of the reduced frequency and the non-dimensional plunge amplitude (kh). These different wake formations can be seen from Figure 1.8.

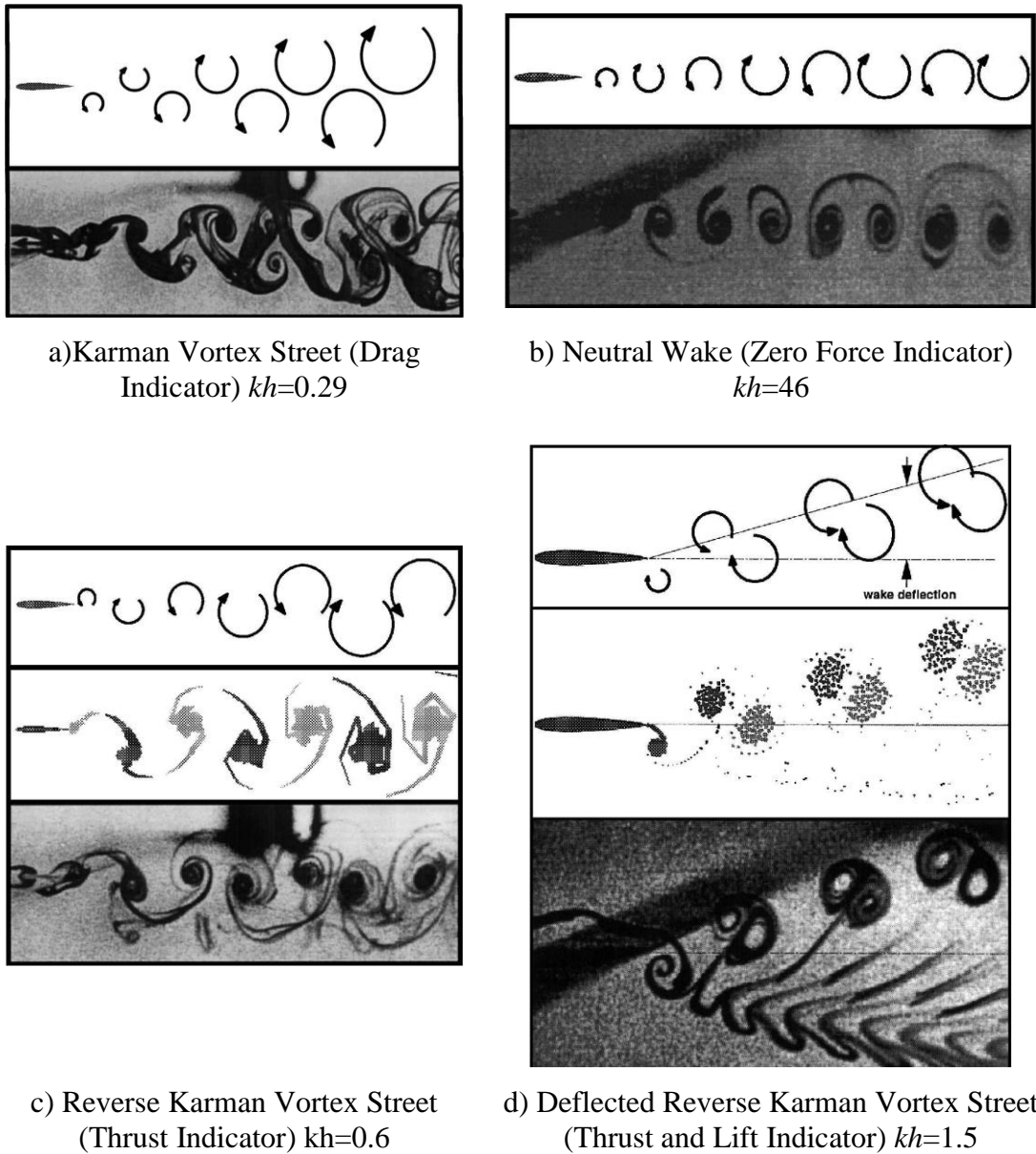


Figure 1.8 : Different Wake Configurations Depending on the Plunging Velocity (kh) (adopted from Jones et al., 1998).

In that study, Jones, Dohring and Platzer (1996) investigated the wake structure behind the plunging airfoil using both numerical and experimental methods. An unsteady potential flow code which is developed at Naval Post Graduate School is used for numerical solution and experiments are accomplished at a water channel using LDV. They showed that experimental results agree well with the numerical results over a wide range of plunging frequencies and plunge amplitudes except at low plunge velocities where viscous effects become dominant and at high plunge velocities where flow separation starts to dominate the flow. In that study, they classified the vortex formations according to the reduced frequency (k) and non-

dimensional plunge amplitude (h) of the plunging wing. Then, they revealed the values of k and h for generating the thrust producing wake which can be seen from Figure 1.9.

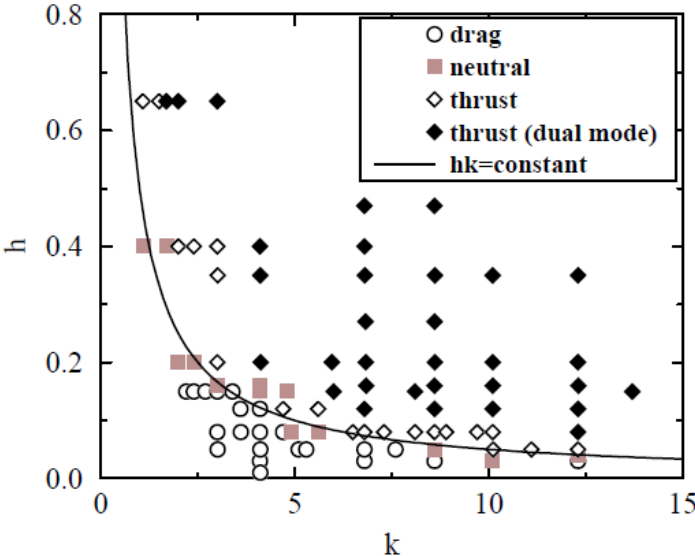


Figure 1.9 : Drag/Thrust as a Function of h and k (adopted from Jones et al., 1996).

Lai and Platzer (1999) visualized the flow field downstream of a NACA 0012 plunging airfoil in a water tunnel using dye-visualization and Laser Doppler Velocimetry (LDV) techniques. They observed that drag producing wake structure (Karman Vortex Street) turns into thrust producing jet flow (Reverse Karman Vortex Street) just after the non-dimensional plunge velocity (kh) exceeds approximately 0.4 value (Figure 1.10). They also showed that this conversion does not occur smoothly. As a result, they stated that the maximum jet velocity is a strong function of the non-dimensional plunge amplitude (h).

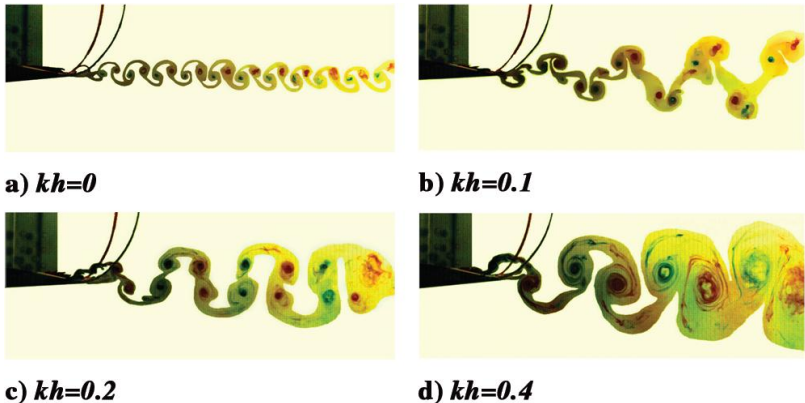


Figure 1.10 : Transition from Normal to Reverse Karman Vortex Street with Increasing kh (adopted from Lai and Platzer, 1999).

Garrick (1936) showed that although pure pitching airfoils generate thrust force above a critical frequency, all plunging airfoils generate thrust force (regardless of their flapping frequency) at all frequencies. Additionally, he used Theodorsen's (1934) inviscid, incompressible, oscillatory flat plate theory to determine the amount of thrust force.

Ho et al. (1980) studied on the velocity field of a NACA 0012 plunging airfoil's unsteady wake using a hot wire anemometry at a low turbulent wind tunnel. According to the experimental results and considering the characteristics of the wake structure, they separated the near wake region as a laminar and a turbulent portion.

Freymuth (1988) has conducted flow visualization experiments in a wind tunnel to observe the propulsive vortical signatures to understand how pure plunging and pure pitching motions (at different reduced frequencies) changes the vortical structure behind the NACA 0015 airfoil. He observed that pure pitching and pure plunging motions produce a reverse Karman Street which generates thrust (producing jet-like flow) behind the oscillating airfoil. Additionally, effects of decrement of the reduced frequency to wake region is observed. Experimental results showed that a decrement in reduced frequency results in increment of the distance between the vortices and at very low frequencies, propulsive tendencies get overwhelmed by the drag of the airfoil profile.

A 2D Navier-Stokes solver is used by Wang (2000) in order to investigate the flow structure around 2D elliptical plunging airfoil and to select the most suitable flapping frequency for forward flight. She investigated the flapping frequency at which both the leading edge and the trailing edge vortices shed from the airfoil and generate optimum thrust or optimum efficiency interacting each other. Lewin and Haj-Hariri (2003) modeled the thrust generation of a 2D sinusoidally heaving airfoil in a viscous flow numerically in order to investigate the flow characteristics and power coefficients of it. They determined both periodic and aperiodic solutions are discovered that for some cases, flow characteristics is not a mirror image of each other during the upstroke and downstroke motions (flow is not symmetric). They realized that the maximum efficiency occurs at an intermediate heaving frequency. Additionally, they categorized the interaction between the leading edge and the trailing edge vortices. Then, the effects of the interactions on system's efficiency are discussed. Young and Lai (2004) simulated the wake of a two dimensional NACA

0012 plunging airfoil numerically using a 2D compressible Reynolds Averaged Navier-Stokes solver making completely laminar and completely turbulent flow assumptions at a certain Reynolds number. The results are well-matched with the experimental wake visualizations in the literature for which the case of flow is assumed completely laminar. They also showed the dependency of the wake structures and the lift and the thrust of the plunging wing to the Strouhal number and the reduced frequency. Winde, et al., (2004) investigated the transitional flows around plunging airfoils numerically calculating them for steady and unsteady onset conditions using a Reynolds Averaged Navier-Stokes method. They found the transition location using the e^N method combining it with a linear stability solver. The obtained numerical results are compared with hot wire pressure and PIV measurements of laminar separation bubbles.

Oo, et al., (2004) investigated the wake structures of a sinusoidally heaving elliptical airfoil in a re-circulated water channel using PIV at a certain Reynolds number and they revealed the thrust producing frequency interval at that Reynolds number.

Miao and Ho (2006) examined the effects of flexure on aerodynamic propulsive efficiency of a plunging flexible airfoil numerically. They simulated the flow structure of the plunging flexible airfoil for various combinations of Reynolds number, reduced frequency and different flexure amplitudes using conformal hybrid meshes. The deformation mods of the flexible flapping wing are illustrated using the dynamic mesh technique. They revealed the strong relation between the propulsive efficiency and reduced frequency. They also determined the highest propulsive efficient Strouhal number and flexure amplitude. Young and Lai (2007a) simulated the flow over a NACA 0012 sinusoidally plunging airfoil using two dimensional Navier Stokes solver at a certain Reynolds number.

Heathcote and Gursul (2007) worked on the jet switching phenomenon for a periodically plunging flexible airfoil in still water using PIV and LDV techniques and they revealed that thrust producing jets behind plunging airfoil deflect periodically in a way similar to flapping shear layers. They also pointed out that switching period changes up to the plunge frequency, plunge amplitude and the stiffness of the airfoil. Lua, et al., (2007a) have been investigated the wake structures of 2D elliptical airfoil undergoing sinusoidally heaving motion in a recirculating water channel via digital particle image velocimetry (DPIV) technique. They pointed

out that drag or thrust production of the system is related to the interaction between the leading edge vortices and the trailing edge vortices. Von Ellenrieder and Pothos (2007) have been examined the flow behind a two dimensional heaving NACA0012 hydrofoil in a recirculating water channel using PIV technique. They asserted that strong vortices can be created at higher Strouhal numbers and they dissipate most rapidly.

Heathcote et al. (2008) examined the effects of spanwise flexibility on flapping wing propulsion by conducting experiments. They visualized the flow structure of a rectangular plunging wing having certain amount of flexibility at a water tunnel via PIV technique and measured the thrust and the lift forces on it with a force balance. They found out that while a degree of spanwise flexibility results in a small increase in thrust coefficient and a small decrease in power-input requirements (leads to a higher efficiency), a pretty greater degree of spanwise flexibility leads to reduced thrust coefficient and reduced efficiency since a large phase delay of wing tip displacement cause a weak and fragmented vorticity pattern. Rival et al. (2008) investigated the influence of airfoil kinematics on the formation of leading edge vortices experimentally using Particle Image Velocimetry (PIV). They found out examining the vortex pinch off process that the deferment of inception and development of leading edge vortex during the dynamic stall is arise from the asymmetric and peak-shifted plunge motions. As a result, they pointed out that tuning the airfoil kinematics carefully may stabilize the leading edge vortex.

Chandar and Damodaran (2008) has been investigated the rigid body dynamics of a NACA 0015 plunging airfoil in incompressible low Reynolds number flow regime by solving the unsteady incompressible Navier-Stokes equations on moving overlapping meshes. They showed that the sharpness of the airfoil's trailing edge has a special importance on thrust generation and airfoils having sharper trailing edges travel faster than the airfoils having rounded ones.

Percin (2009) examined the interaction between the leading edge and the trailing edge vortices for various reduced frequencies and non-dimensional plunge amplitudes both numerically and experimentally. Digital Particle Image Velocimetry is used during the experiments and CFD Package Fluent is employed for the numerical calculations. The consistency of experimental results with numerical simulations is shown in the study. As a result, he pointed out that, wake formation is

affected by the interaction between the leading and the trailing edge vortices. Drag or thrust is produced depending on the interaction. According to this study, thrust coefficient and propulsive efficiency depends on both the reduced frequency (k) and product of the reduced frequency and the non-dimensional plunge amplitude (kh). The combined experimental and numerical results of this study is summarized in Figure 1.11.

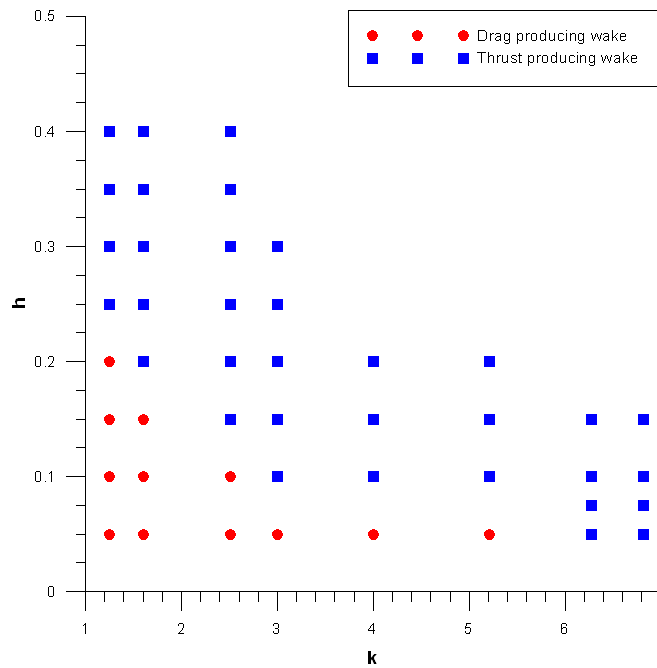


Figure 1.11 : Wake Configurations as a Function of Reduced Frequency (k) and Non-dimensional Plunge Amplitude (h) (adopted from Percin, 2009).

Pitching motion is another important research interest among the researchers therefore pitching airfoils are investigated in several studies both numerically and experimentally.

Koochesfahani (1989) investigated the vortical patterns in the wake of a pitching NACA 0012 airfoil and controlled the thrust/drag generation mechanism by changing the frequency and amplitude of the oscillation. Experiments are conducted in a low speed water channel using Laser Doppler Velocimetry (LDV) technique oscillating the airfoil sinusoidally and non-sinusoidally. He also compared the consistency of the experimental results with the previous numerical results.

Sun and Sheikh (1999) tried to surpass the dynamic stall for an oscillating NACA 0012 airfoil (making pitching motion) using steady and unsteady tangential blowing techniques. They modeled and solved the problem numerically by solving Reynolds

Averaged Navier-Stokes Equations and revealed that the unsteady blowing is more effective than the steady blowing. Hamdani and Sun (2000) analyzed a pitching NACA 0012 airfoil performing at low Reynolds number numerically by solving the 2D Navier-Stokes Equations in order to predict the unsteady force production of the airfoil which accelerate or decelerate from one transitional speed to another and rapidly pitching up in constant free-stream. They also examined whether airfoil lift coefficient is smaller and the drag coefficient is much larger than that in the high Reynolds number rather than the low Reynolds number or not.

Jung and Park (2005) investigated the characteristics of Karman vortex shedding in the near wake of pitching NACA 0012 airfoil in a small open-circuit wind tunnel using smoke wire flow visualization and hot-wire measurements. They found that the shedding frequency in the wake of oscillating airfoil is much different from the case of the steady airfoil at a given angle of attack.

Guvernuyuk and Dynnikova (2007) modeled the unsteady flow over a NACA 0012 airfoil making angular oscillations in a viscous incompressible flow and solved it numerically using the Lagrangian vortex method to solve the Navier-Stokes equations. They determined the unsteady forces on the airfoil and vorticity field; then the numerical results are compared with the experimental results. This study enables to analyze the hydrodynamic mechanism of generation of time-dependent loads on an oscillating wing.

While some of the studies focuses on purely plunging or purely pitching airfoils in order to understand the distinctive effects of each on thrust mechanism, some studies investigates the combinations of them to generate a synchronization between these motions.

Anderson and coworkers (1998) conducted experiments to investigate the characteristics of the flow around and in the wake of the oscillating airfoil. They visualized the flow structure around a NACA 0012 airfoil using DPIV at Reynolds number 1100. Additionally, force and power measurements are accomplished at Reynolds number 40000. The experimental results' compatibility with theoretical predictions of linear and nonlinear inviscid theory is also compared. As a result, they revealed the optimal thrust generating conditions ($0.25 < St < 0.40$ and AOA_{max} : large maximum angle of attack $15^{\circ} < AOA_{max} < 25^{\circ}$). They also observed that strong leading

edge vortex can lead to thrust generation interacting with the trailing edge vortex. Finally, significance of the phase angle between the pitching and the plunging motions on maximizing the propulsive efficiency is revealed. Read et al. (2003) also conducted experiments on a harmonically pitching and heaving NACA 0012 airfoil in the MIT Department Ocean Engineering testing tank in order to determine the most suitable thrust producing parameters. They found out that the phase angle should be between 90° - 100° to attain the best thrust performance. They also showed that a sinusoidal variation in angle of attack enables attaining much higher thrust coefficients at high Strouhal numbers. Additionally, testing the airfoils with superimposed pitch bias and impulsive start in still water, they observed that, harmonically oscillating airfoils provide large lateral forces for maneuvering capabilities. Von Ellenrieder, et al. (2003) examined the three dimensional structure of the flow behind a pitching and heaving finite span wing using dye flow visualization at a constant Reynolds number ($Re=164$) in a re-circulating water channel. The 3D flow and vortex structure is constructed combining two orthogonal views and sequencing them. They showed the effects of the variation of the Strouhal number pitch amplitude and heave phase angle to the structure of the wake.

Lu et al. (2003) investigated the propulsive performance and vortex shedding of an elliptical wing section conducting pitching and plunging motion using 2D Navier-Stokes solver. The three different types of leading edge vortex shedding evolution are identified in this study. They also discussed the relation of the thrust and the drag force behavior with vortex structures near the airfoil and vortex shedding at the near wake region. Additionally, effects of several parameters (frequency, amplitude of oscillation, phase difference, thickness ratio of the airfoil) on the vortex shedding and force generation mechanism are examined. Guglielmini and Blondeaux (2004) examined the flow around a NACA 0012 pitching and plunging airfoil having a steady forward motion by solving numerically the momentum and continuity equations using a stream-function vorticity formulation at two different Reynolds numbers. They compared the results with the previous experimental measurements in order to prove the consistency of numerical and experimental results. Additionally, the force and the torque acting on the foil are computed. They pointed out that when pitching and plunging motions are combined in a steady forward motion, the foil produce much larger values of thrust and better efficiencies.

Schouveiler et al. (2005) conducted a sequence of experiments in a tow tank to investigate the effects of variations of Strouhal number and maximum angle of attack on a harmonically pitching-plunging NACA 0012 airfoil's thrust force and its hydro-mechanical efficiency using dye flow visualization technique. They determined the combination of parameters providing optimum efficiency (70%). They have also identified a parameter range where the propulsive system achieves high efficiency and high thrust.

Windte, et al. (2005) investigated numerically the flow around the NACA 4402 airfoil simulating the conditions for steady onset as well as pure plunge and a combined pitch plunge motion using a Reynolds Averaged Navier-Stokes solver (RANS). They found out that combined pitch and plunge motion is essential to obtain high propulsive efficiencies. Anttonen, et al. (2005) has been used the multi-POD (Proper Orthogonal Decomposition) technique to solve the 2D flow around a NACA 0012 pitching and plunging airfoil and they showed that this technique represent a reasonable level of accuracy for design.

Fuchiwaki and Tanaka (2006) visualized the flow around a pitching and a heaving airfoil at a water channel in a low Reynolds number region using dye flow and Schlieren visualization techniques in order to clarify the vortex structure and vortex scales on it.

Yang et al. (2006) optimized a sinusoidally pitching and plunging NACA 0012 airfoil for high propulsive efficiency and for high time averaged thrust coefficient using inviscid version of a 3D unsteady compressible Euler/Navier-Stokes flow solver. After determining the highest propulsive efficiency and time averaged thrust coefficient they found out that mean angle of attack's effect on this parameter is negligible. Young et al. (2006) investigated the effects of flow separation on the thrust and efficiency of a pitching and plunging airfoil in various combinations using a 2D unsteady Navier-Stokes solver. They validated their numerical results with experimental flow visualization results for plunging; numerical studies for pitching motions. Additionally, combined pitching-plunging motions are also computed via solver and results are compared to Garrick's (1936) small amplitude potential theory, large amplitude unsteady panel method potential flow simulations (Young, Lai 2004) and Anderson et al.'s (1998) experimental results. They showed their results' consistency with previous results and stated that leading edge separation should be

minimized in order to get the highest efficiency propulsion. Young and Lai (2007b) simulated a pitching and plunging NACA 0012 airfoil using two dimensional Navier-Stokes flow solver to determine the mechanisms influencing the efficiency of oscillating airfoil propulsion and they compared the numerical results with previous experimental studies, an inviscid analytical method and an unsteady panel method code. Lian and Shyy (2007) investigated the effects of plunging amplitude and reduced frequency on force generation for a plunging NACA 0012 airfoil by conducting Navier-Stokes computations and compared the numerical results with the literature. They also made numerical solutions for combined pitching and plunging case focusing on the impact of Strouhal number on the force generation. Additionally, the influence of gust on the combined pitching-plunging wing is examined. They found out that at a fixed flapping frequency, increasing the plunging amplitude can make the airfoil from drag to thrust generating. Finally, they also showed that flapping airfoils are gust resistant since they can smooth out the large free stream velocity variations.

Lua, et al. (2008) has been investigated the effects of flapping angle and frequency on aerodynamic force characteristics of a 2D heaving wing in a recirculating water channel in assistance with a force sensor. They also related them to the associate flow field which is obtained via digital particle image velocimetry. Srigrarom and Vincent (2008) determined the best flapping motion combination for a pitching and plunging SD8020 hydrofoil mimicking the flapping and swimming motion of the marine creatures making force and torque measurements and dye flow visualization in the water tunnel at low Reynolds number. They determined the optimum pitching amplitude, angular frequency and Strouhal number at a certain Reynolds number. Thus, the best conditions for thrust production at low Strouhal and Reynolds numbers is determined. Fenercioglu and Cetiner (2008) are also investigated the flow structure around a combined pitching and plunging SD7003 airfoil which is optimized for flows with large separation bubbles using Digital Particle Image Velocimetry (DPIV) for Reynolds numbers 2000 and 27500. They commented the thrust or drag production of the airfoil examining the flow visualization data.

Isaac et al. (2008) investigated a thin chambered semi-elliptic harmonically pitching and plunging plate airfoil's flow structure and thrust generation simulating it with a CFD solver, visualizing the flow structure via PIV and measuring the forces on the

airfoil via a force transducer at a water tank. According to the experimental results, leading edge/trailing edge switching makes it feasible to use insect chambered wing in order to increase the performance when dynamic chamber control is not applicable.

Brunton, and co-workers (2008) have investigated the unsteady forces on low-Reynolds number pitching – plunging flat plate using 2D and 3D numerical simulations and wind tunnel experiments to develop low order dynamical system models for the unsteady lift and drag forces on small wings in various modes of flight and to better understand the physical characteristics of unsteady laminar separation.

While developing new technologies or vehicles, mankind generally inspired from nature and existing vehicles. Since reverse engineering has an important place on new systems' development, some of the researchers examined both animals and existing micro air vehicles.

Bomphrey (2006) states that scientist are inspired from the nature while they are developing micro air vehicles (MAVs). They solved the design problems for several mission such as load carrying, hovering, observing and mimicking the mission specific structure of the insects.

Blondeaux, and co-workers (2005) have made numerical solutions in order to simulate the flapping foils mimicking the fish-like locomotion and compared the results with previous flow visualization studies. They found out that a vortex ring is shed by the oscillating foil every half a cycle and dynamics of these rings depend on the Strouhal number. Ansari, et al. (2006) have modeled an insect-like flapping wing developing two novel coupled nonlinear and wake integral equations and solving them using numerical methods in order to determine the forces and the moments on the wing via a Fortran code. Best values for numerical parameters are determined by making a sequence of numerical experiments. The numerical results are compared with the existing experimental data and consistency of the numerical results with the experimental results is shown. The model also showed the similarity between 2D and 3D flows for insect like flapping wings at low Reynolds number.

Hong and Altman (2007) investigated the contribution of streamwise vorticity to the total measured lift for a flapping wing micro air vehicle. The lift generated by

flapping wings is measured via force transducer and a high speed camera. The contribution of streamwise vorticity to the total lift is determined using Digital Particle Image Velocimetry (DPIV). They pointed out the importance of the relationship between the wing span and the flapping frequency. Muijres et al. (2008) observed via DPIV technique that a small nectar feeding bat can 40% increase the lift force exerted on its wing by means of attached leading edge vortices during slow forward flight. They also found out that the bat's maximum lift coefficient value can reach up to 4.8 since the airflow passing over the leading edge vortex (LEV) smoothly reattaches to the wing behind it. That's why; the bat can fly exceptionally large local angles of attack.

Many studies have also been conducted on oscillating wings and flat plates. Yadykin, and coworkers (2003) examined the fundamental properties of the added mass of a plane flexible plate oscillating in a fluid by numerically. They found out that an increase of the order of the mode of vibration decreases the added mass. Additionally, a decrease in aspect ratio results in a decrease of added mass. Sarkar and Venkatraman (2004) applied System Equivalent Reduction Expansion Process (SEREP) to model order reduction for linear unsteady aerodynamics problem. Two-dimensional incompressible potential flow past on oscillating NACA 0012 airfoil is examined and the results are compared with Proper Orthogonal Decomposition (POD) based reduction in terms of computational cost. As a result, SEREP is found more efficient for the examined linear system case. However, the POD's wide application area (both linear and non-linear systems) stated in order to remind the limitation of SEREP's usage area with linear systems.

Birch and Lee (2005) investigated the downstream development of the 3D flow structure of a tip vortex in the close region just behind the sinusoidally oscillated NACA 0015 airfoil using a triple hot wire probe in the suction-type subsonic wind tunnel at a certain Reynolds number.

Milano and Gharib (2005) observed that the maximum lift is generated after pinching off the leading edge vortex just at the end of the half stroke after execution of a genetic algorithm to their experiments where a rectangular flat plate is flapping with two degrees of freedom in a tow tank.

Ringuette et al. (2007) observed the unsteady vortex formation on one end free normal flat plates having low aspect ratio using DPIV at a towing tank. Visualization the three dimensional flow structure around flapping flat plates, they found that tip vortex has a significant contribution on plate forces. They also added that eliminating the tip vortices leads to a force minimum on flat plates. Additionally, it can be said according to the experimental results that drag coefficient inversely proportional to the aspect ratio of the flat plates.

Experimental methods can also be used in order to measure airfoil's certain specifications. Windte, and coworkers (2006) investigated the flow around a SD7003 static airfoil having an angle of attack and laminar separation bubble on it using both numerical and experimental methods and the results are compared at a certain Reynolds number. A Reynolds Averaged Navier Stokes solver (RANS) is used in order to simulate the flow numerically and the 2D Particle Image Velocimetry (PIV) measurements are conducted at the upper surface of the airfoil to visualize the flow experimentally. They also compared their results with XFOIL program. Van Oudheusden, Scarano and Casimiri (2006) examined the non-intrusive load characterization of a NACA 642A015 airfoil. They obtained the flow field information and the mechanical loads by making control volume approach and using Particle Image Velocimetry (PIV) technique. They combined the data coming from control volume approach and PIV measurements and validated it with CFD results.

The gathered information from studies about flapping wings directed researchers to development of efficient Micro Air Vehicles. Since these devices have to consist of more than one airfoil, researchers have been conducting studies analyzing the interaction of two objects in order to understand the effects of interactions on thrust mechanism.

Tuncer and Platzer (1996) investigated the thrust generation of a single flapping airfoil and a flapping/stationary airfoil combination in tandem using a multi-block Navier-Stokes solver. They revealed that the propulsive efficiency of the system is strongly depending on the reduced frequency and amplitude of the flapping motion. Conducting numerical studies, they determined the flapping airfoil's propulsive efficiency as 70% (at certain flapping amplitude and certain reduced frequency). Above all, they also observed 40% propulsive efficiency augmentation for the airfoil combination in tandem case (at increased reduced frequency and decreased plunging

amplitude). The research showed that the stationary trailing airfoil augments the thrust at relatively high reduced frequencies.

Jones and Platzer (1999) conducted studies about flapping wing propulsion. They used several configurations to investigate the effects of interaction of oscillating wings to thrust production. Experiments are conducted at low speed wind tunnel and Laser Doppler Velocimetry is used during the data acquisition process. A mechanical system is developed and produced for simulating pitch and plunge motions. They have also made numerical calculations using unsteady panel code for same configurations and compared the results with the experimental ones.

Lan and Sun (2001) investigated the aerodynamic force and flow structures of two flapping airfoils in tandem configuration solving the Navier-Stokes equations. They examined the three typical phase differences between the fore and the aft airfoil. According to the numerical results, the largest vertical force is generated during the inphase flapping case and the largest horizontal force is produced during the 90 degrees phase difference flapping case. Kaya and Tuncer (2004) have made an optimization study in order to getting the maximum thrust and propulsive efficiency from an oscillating wing couple (in counter-phase) seen in Figure 1.12. They revealed the best phase angle between pitching and plunging motions for a certain reduced frequency using a Navier Stokes solver which enables to examine the viscous compressible flows.

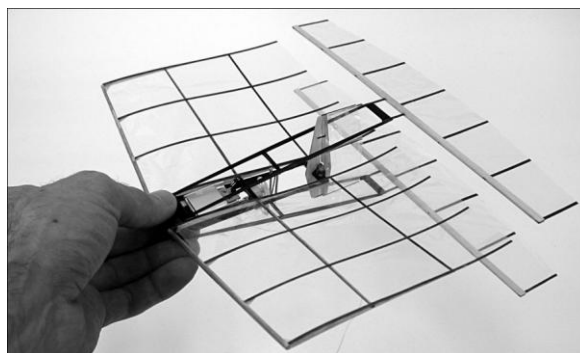


Figure 1.12 : Dual-Flapping MAV (adopted from Kaya and Tuncer, 2004).

Zhang, et al. (2005) investigated the aerodynamic loading on a cylinder behind a NACA 4412 fixed airfoil in a low speed wind tunnel using a load cell and a hot wire. They found out that unsteady forces on the cylinder depends on the lateral distance between the airfoil and the cylinder and depends on the Reynolds number.

Experimental results showed that lateral distance and unsteady forces are inversely proportional with each other. They also explained that airfoils' vortex makes a significant contribution to the forces on the cylinder up to a certain Reynolds number. Above it, unsteady forces on the cylinder is only generated due to its own vortex shedding.

Han and Cho (2006) examined the fluid propulsion mechanism of two oscillating flat plates numerically combining a core addition scheme and a vortex core model. They investigated closely coupled aerodynamic interference between flat plates calculating their wake structure for heaving and pitching motion separately. They also compared the numerical results with experimental fluid visualization results. Additionally, they plotted the velocity contours at a certain distance after the pitching flat plates for several frequencies in order to examine the thrust generation mechanism. Han et al. (2008) investigated the propulsive characteristics of dual fish-like foils examining the effect of vertical and horizontal distances between the foils using unsteady panel method and validating it with other numerical and experimental data. Observing the vortical interaction for different foil positions, they found out that the leading foil's propulsive characteristics change only a little with the vortical distance contrary to the following foil whose propulsive characteristics are strongly depend on the vertical and horizontal distance between them. As a result of the numerical analysis, they showed that while the entire wake structure depend mainly on the horizontal distance, the intensity of the mutual interaction between wake vortices depend on the vertical one. Therefore, it can be easily said that the propulsive characteristics of dual-fish like foils are strong functions of the vertical and horizontal distances between them.

Many of the studies investigating vortical interaction mechanism have been conducted using mainly numerical methods since examining this issue with experiments requires a serious foundation, hardware and experimental setup. In this study, the effects of tail location and tail angle on plunging wing's thrust or drag production is examined using Digital Particle Image Velocimetry (DPIV) Method in order to assist the development of new generation more efficient Micro Air Vehicles.

2. EXPERIMENTAL SETUP AND DATA ACQUISITION

2.1 Flow System

Experiments were conducted in a re-circulating large scale water channel located in the Trisonic Research Laboratory at the Faculty of Aeronautics and Astronautics of Istanbul Technical University. The water channel mainly consists of three tests sections each has a dimension of 1010 mm x 790 mm, a reservoir, a sink, a set of honeycomb and five screens in order to decrease the turbulence intensity level and providing a uniform flow for test section. Figure 2.1 shows the channel's CAD drawings and photos from different aspects.

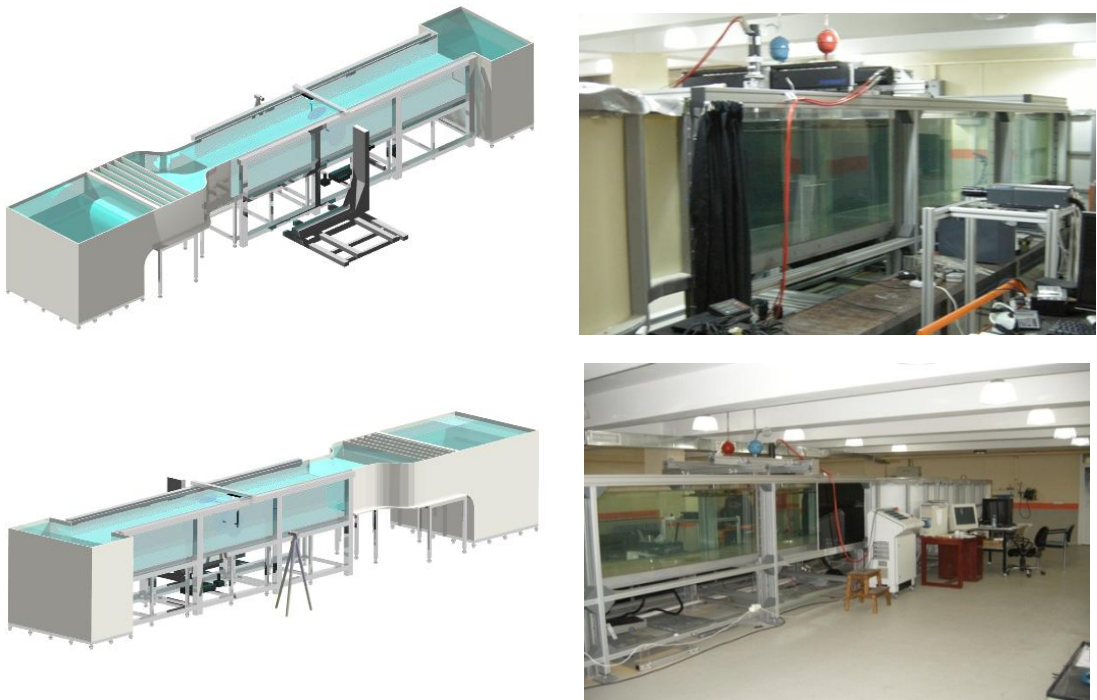


Figure 2.1: Large Scale Water Channel.

Since the water quality in channel has significant effects on experimental results, special filtration systems are used. After the filtration of the city water it fills to an external tank and, it is filtered several times with a certain time interval. Then, the water in the external tank passes a sequence of external filters before filling the water channel. These filters can be seen from Figure 2.2-a.



a) External Filters



b) Centrifugal Pump

Figure 2.2 : External Filters and Centrifugal Pump.

14 tons of water is circulated by a centrifugal pump (Figure 2.2-b) in the water channel. Water is pumped to the reservoir section and therefore it is forced to flow through the contraction section passing through the honeycomb and five screens. Accelerating at the contraction section by means of narrowing, water flows through the three test sections and comes to the sink. Then, it is sent back to the reservoir again by means of the centrifugal pump.

Test sections' sidewalls and bottom wall are made of thick transparent Plexiglass panels in order allow data acquisition via optical techniques like Digital Particle Image Velocimetry and Laser Doppler Anemometry (LDA) etc.

The adjustment of the water channel's velocity can be done with a controller seen in Figure 2.3 adjusting the RPM (revolutions per minute) of the centrifugal pump.



Figure 2.3 : Controller of the Centrifugal Pump.

In order to determine the suitable RPM value for a certain free-stream velocity, calibration equation written in Equation (2.1) is used.

$$U_{\infty} = 0.0912(RPM) + 1.0478 \quad (2.1)$$

Where U_{∞} is the required free stream velocity in terms of mm/s and RPM is the centrifugal pump's turning speed in terms of RPM. Equation (2.1) is only valid for the condition that the water depth in the test section is 713 mm. Since the height of the water column in the test section is inversely proportional to the water channel's speed for the same RPM value of the pump, any increment of water column's depth results in an decrement of the water channel's speed. Therefore the height of the water column in the test section was arranged carefully before the experiments. The approximate maximum speed of the re-circulating water channel is 0.137 m/s.

In this study, experiments are performed at the free stream velocity of 0.05 m/s and 0.1 m/s. Therefore the RPM values corresponding to these velocities are calculated as 536.7 and 1085 respectively.

2.2 Experimental Models and Montage

Experiments were carried out using a plunging NACA 0012 airfoil with a span of 30 cm and a chord length of 10 cm and a NACA 0012 tail with a span of 31 cm and a chord length of 5 cm. Both of the plunging wing and the tail are made of Plexiglas by CNC milling machine in order to allow the laser light to illuminate both sides of it and they are also painted in black except a plane where laser sheet have to pass through them. Additionally, a flat plate having same dimensions with the tail is also produced by laser cutting. Figure 2.4 shows the images of the wing, tail and the flat plate.

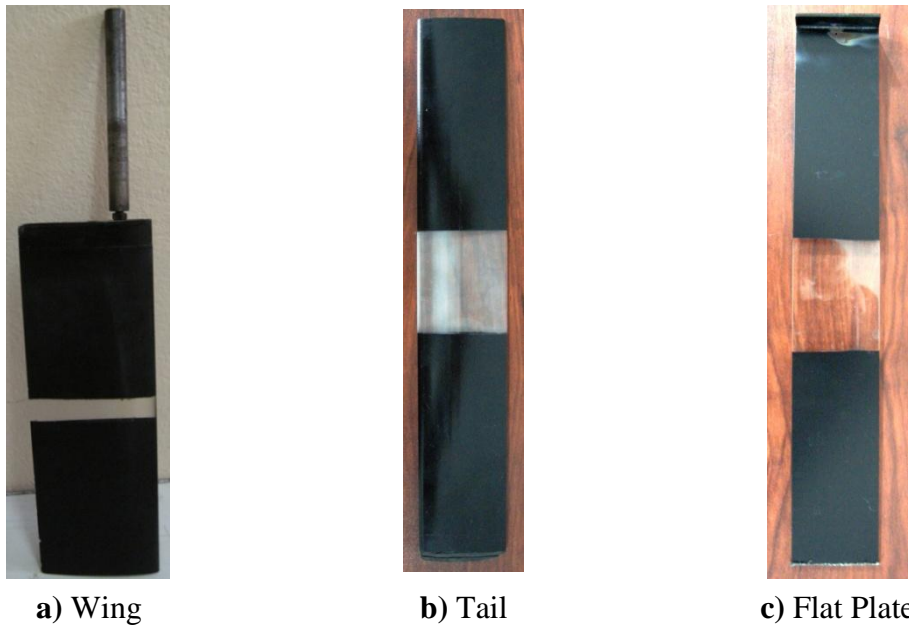


Figure 2.4 : Images of Wing, Tail and Flat Plate.

In order to clamp the flat plate to the upper end-plate and for locating it to different distances from the trailing edge of the wing, a ruler and C shaped support is produced.

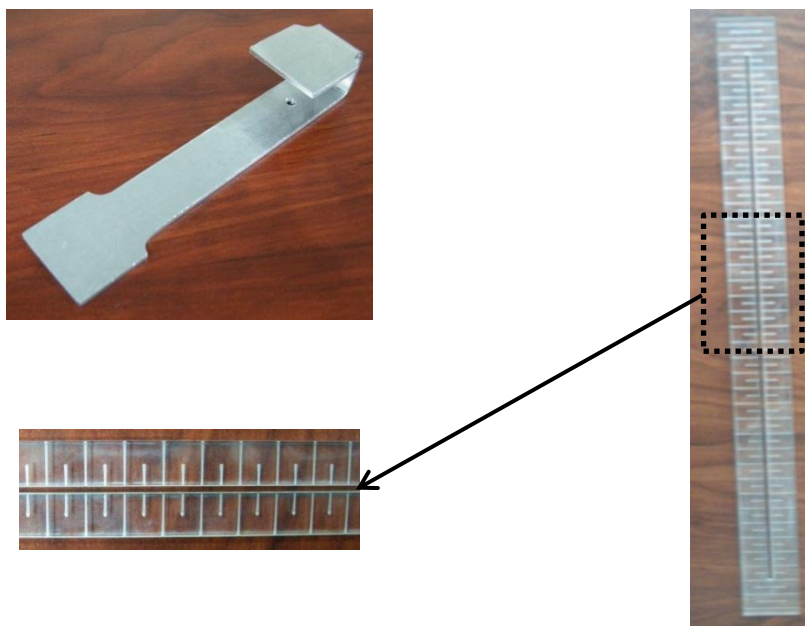


Figure 2.5 : Images of the Ruler for Flat Plate and C Shaped Support.

Additionally, 2 special rulers (Figure 2.6) are produced in order to arrange the angle of the tail airfoil to 15 degree and 30 degree.

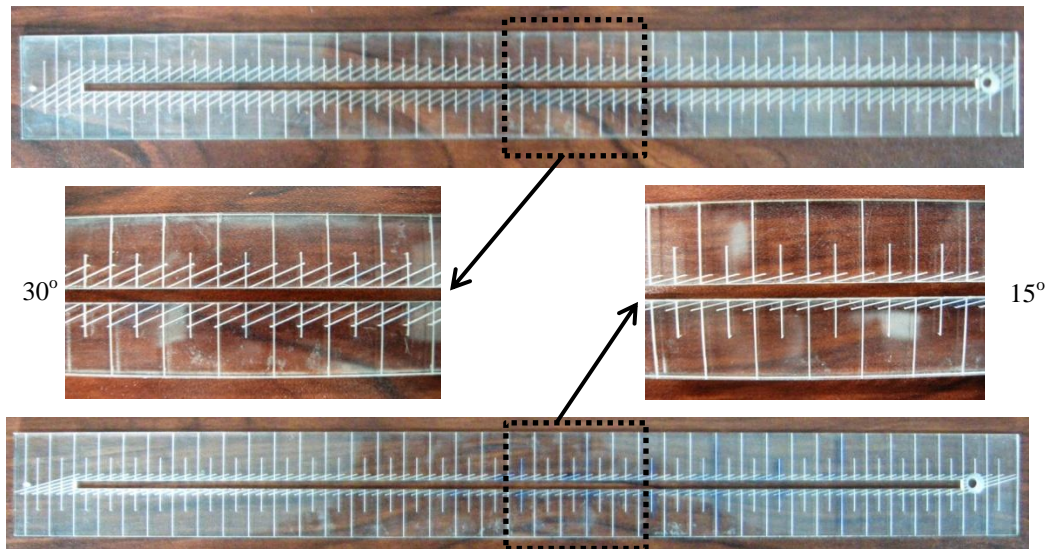


Figure 2.6 : Images of the Rulers for Tail Montage.

The wing shown in Figure 2.4-a is mounted vertically to servo-motor's extension from its shaft location at quarter chord. The suitable ruler – C support couple are combined and fastened to the upper endplate in order to mount the tail or the flat plate and can arrange tail's angle of attack. Additionally, positions of both the tail and the flat plate are arranged via these rulers. Rulers have been pulled through the upper end-plate via a fish line to prevent the prolapse due to the gravity. Both the flat plate and the tail are fixed between the upper and lower end-plates for different experiments with the assistance of non-skid fabric which glued to the bottom of both the tail and the flat plate carefully in order to prevent any movement of these objects. Since lower end-plate is hanged from the upper end-plate, it is supported with special foams to prevent the effects of flow induced vibrations on it. Figure 2.7 shows the montage of the wing – the flat plate combination and similar types of montages were made for experiments accomplished with tail.



Figure 2.7 Montage of one of the Experimental Cases

A special grid seen in Figure 2.8 is produced for calibration process. It can be located between the wing and the tail or flat plate easily.

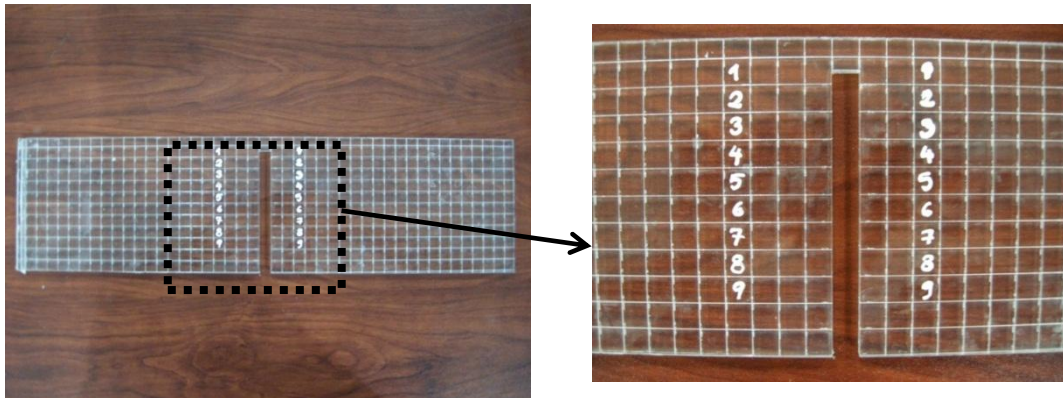


Figure 2.8 : Grid.

2.3 Airfoil Motion

Sinusoidal plunging motion of the airfoil is generated by Labview VI (Virtual Instrument) signal generator and transmitted to servo control unit (Figure 2.9).

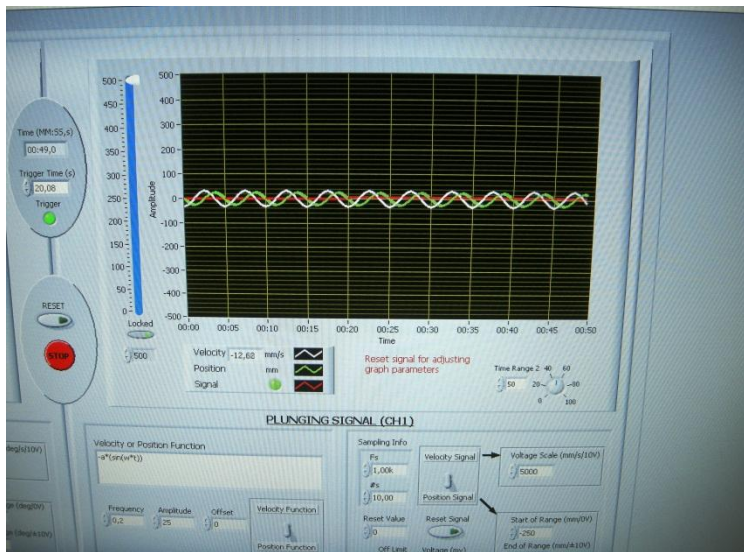


Figure 2.9 : Labview VI.

The program uses the values of plunging frequency, amplitude of the motion and offset in order to generate a signal according to the input function which is: $f(t) = -a \sin(2\pi ft)$. Then, the suitable position function is send to a Kollmorgen/Danaher Motion AKM3E servo motor (Figure 2.10) by servo control unit and airfoil starts plunging motion inside the water channel.

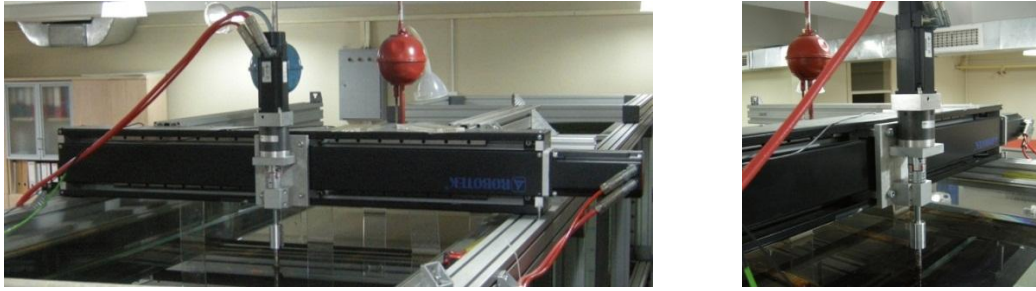


Figure 2.10 : Kollmorgen/Danaher Motion AKM33E Servo Motor and Its Gear System.

The basic properties of the servo motor system are summarized in Table 2.1.

Table-2.1 : Basic Specifications of Kollmorgen/Danaher Servo Motor.

Model of Servo Motor	Continuous Rated Torque (N.m)	Rated Speed (RPM)	Maximum Speed (RPM)
AKM33E	2.34	4500	5490

2.4 Digital Particle Image Velocimetry Method

Digital Particle Image Velocimetry (DPIV) is an advanced optical non-intrusive flow visualization technique that enables observing the flow field of an area measuring the distance traveled by the particles in the flow within a known time interval. Since it is an optical method, the flow is seeded with suitable amount of special particles which will affect the flow field at negligible levels and the investigated area is illuminated with laser beam; then, movement of the particles are recorded by CCD-cameras (Charged Couple Device cameras) focusing on the interested plane. The aim of this effort is to acquire captures which give information about change of the particles' positions on interested area for gathering both the velocity and the vorticity information on that field with completion of the post processing steps. Velocity field of the measurement area is determined by dividing the camera images to rectangular interrogation areas and determining the displacement vectors of them by observing the particles' travel within a known time interval. Each area gives a vector and therefore the velocity field of the interested are can be gathered. After that, vortex structure of the interested flow field can be determined.

In this technique, cameras and laser are synchronized in order to gather accurate results. Therefore the time between pulses of the laser and the trigger rate of the cameras have to be calculated before the experiment. After the data acquisition the

raw data is processed. Therefore, it can be said that the DPIV technique consists of two phases: 1) Data Acquisition 2) Data Analysis.

Figure 2.11 summarizes the basic principle of the DPIV technique.

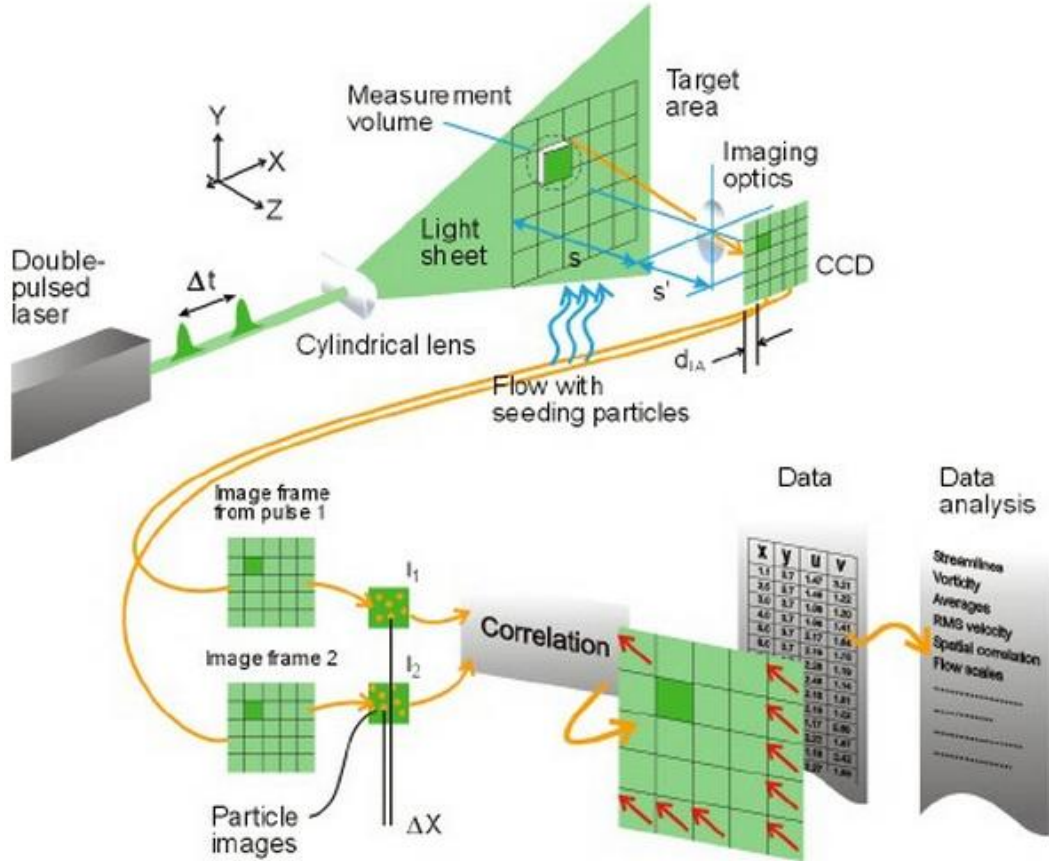


Figure 2.11 : Summary of DPIV’s Basic Principle (Url-1).

The further information about the seeding, recording, illumination, synchronization, correlation, masking, validation and other processes are explained in the following sub-sections.

2.4.1 Seeding

DPIV method requires seeding of the flow in order to tracking the motion of the particles by means of visualization of the interested area. While selecting the suitable seeding material several parameters should be considered since it is affecting the flow structure.

The density of the seeding material should be so close (or same if possible) to the fluid’s density in order to prevent the sinking and buoyancy of the particles and they should be also small for following the flow naturally. Since the measurement area

will be illuminated with the laser, seeding particles should be big enough to reflect the light accurately. They should also be cheap, chemically inactive and non-toxic. The list of seeding materials for liquid flows is represented in Table 2.2.

Table 2.2 : Seeding Materials for Liquid Flows (Cetiner, 2010).

Type	Material	Mean Diameter (μm)
Solid	Polystyrene	10 – 100
	Aluminum	2 – 7
	Glass Spheres	10 – 100
	Granules for Synthetic Coatings	10 – 500
Liquid	Different Oils	50 – 500
Gaseous	Oxygen Bubbles	50 – 1000

Additionally, particle shape has an important effect on particles' behavior in fluid owing to the fact that the drag force on the particle is strongly depend on the geometry of it.

In this study the flow is seeded with “Silver Coated Hollow Glass Particles” having a diameter of $10\mu\text{m}$ and a density of 1.1 g/cm^3 (Figure 2.12).



Figure 2.12 : Silver Coated Hollow Glass Particles.

2.4.2 Data Recording

The illuminated flow structure can be recorded by cameras during the DPIV process. Recent developments in camera technology leads to the usage of digital cameras.

In this study flow images are captured by two 10-bit Flow Sense cameras with 1600×1200 pixels resolution and 30 Hz frame rate shown in Figure 2.13.



Figure 2.13 : Flow Sense Cameras.

2.4.3 Illumination

The illumination of the measured flow area is accomplished by lasers since they have an ability to emit monochromatic light with high energy density.

Two different types of laser systems can be used in DPIV studies: 1) Continuous Lasers, 2) Pulse Wave Lasers. While continuous lasers provide continuous illumination, pulse wave lasers pulses within very short time intervals. Since their costs are much cheaper than the continuous ones, pulse wave lasers are generally used in DPIV experiments.

In this study, the flow illuminated is accomplished by a New Wave Solo-PIV 120 Nd: Yag laser (max. 120 mJ/pulse) with two cavities each one pulses at 15 Hz rate (Figure 2.14).



Figure 2.14 : Dual Cavity Nd:Yag Laser.

2.4.4 Synchronization

Both the cameras and laser should be synchronized with each other for accurate data acquisition. Therefore the timer box is used in order to control both the camera trigger and the laser pulses.



Figure 2.15 : Synchronization of the System (Andersen, 2007).

2.4.5 Correlation

Since DPIV images are analyzed by subdividing the camera image into small rectangular interrogation areas, displacement vectors of the image can be determined by observing the seeding particles from one sample to its counterpart in the second image. Figure 2.16 represents the correlation process that is applied in this study.

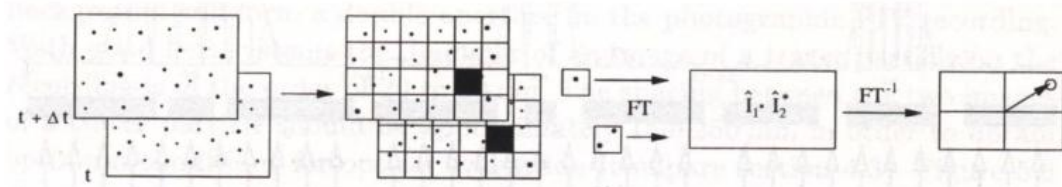


Figure 2.16 : Double Frame / Single Exposure Recordings, The Digital Cross Correlation Method (adopted from Raffel et al, 1998).

2.4.6 Masking, Validation and Other Processes

In the most of the DPIV studies, effect of an object on flow structure is examined. Therefore, the cameras usually record the cross section area of the object with seeding particles in the measurement area. Cross section area of the object should be masked for preventing the generation of incorrect vectors called bad vector. This process is called masking.

After the masking process, there might be also a few bad vectors governing from the insufficient illumination. This can be solved by conducting range validation process where incorrect vectors can be eliminated according to a reference value. A program takes as the reference value as an input and compares the vector magnitudes with it in order to see whether they are meaningful or not. Thus, bad vectors are eliminated via this step. Additionally, different types of filters can be employed the data for reducing the noise in the measurements.

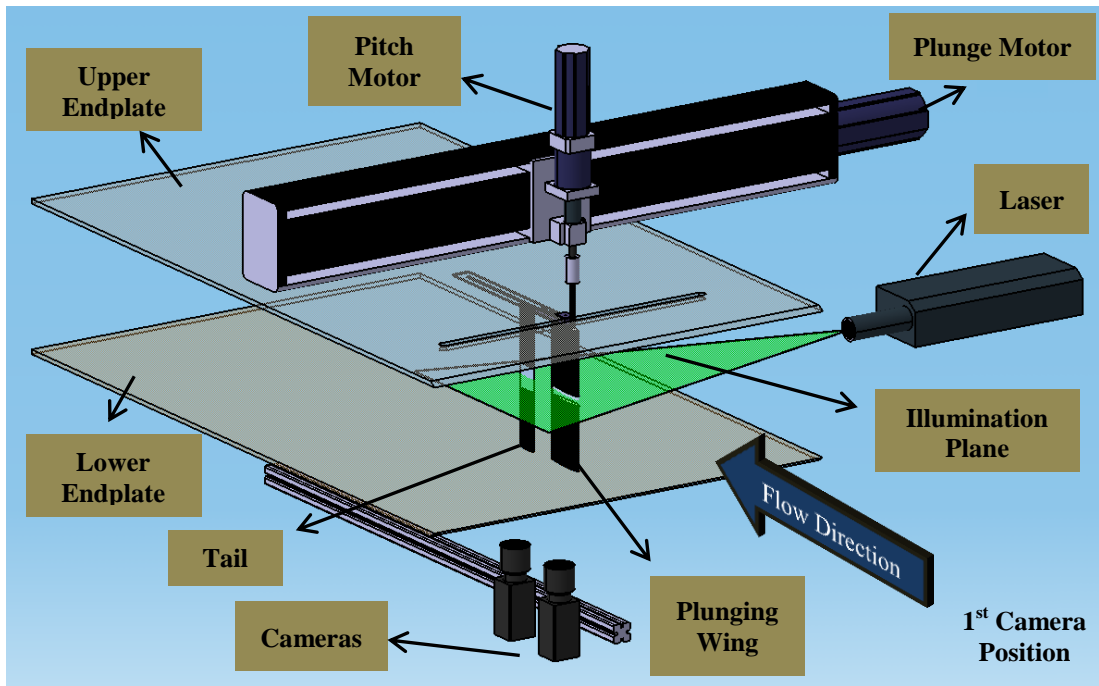
2.5 Experiments

2.5.1 Image Acquisition

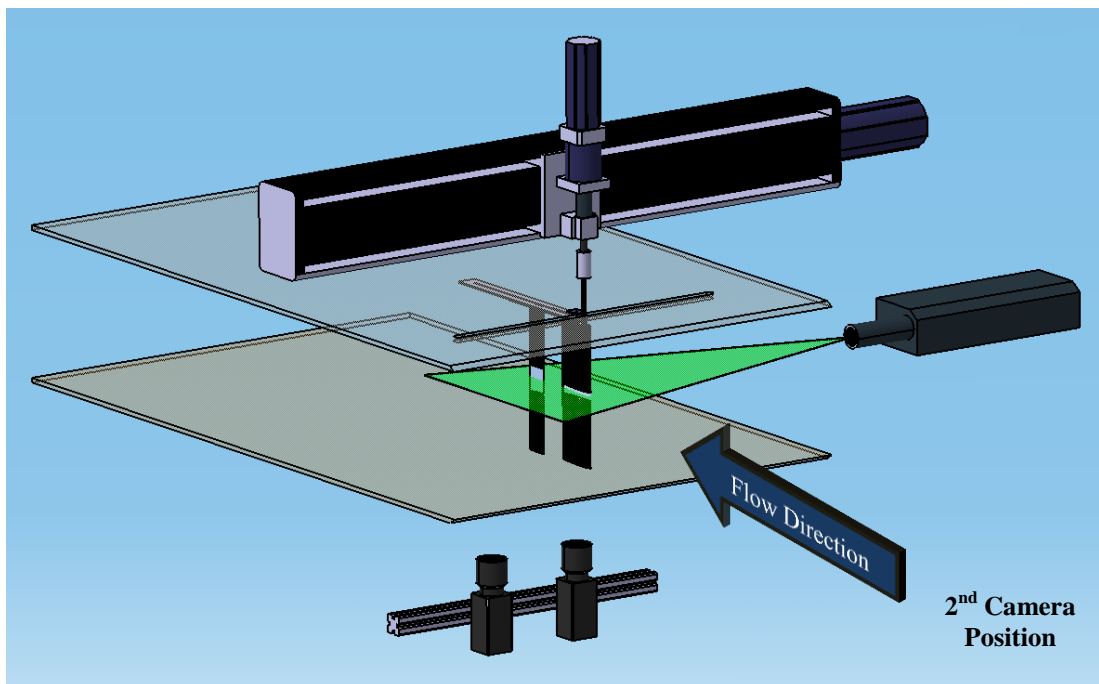
Water channel is refilled with fresh water for getting better DPIV images before the experiments. After that camera arrangements and calibration process is accomplished with the assistance of grid shown in Figure 2.8.

In this study, quantitative flow images are captured via Dantec Dynamics' DPIV system consisting of two Flow Sense PIV cameras, a New Wave Solo-PIV 120 Nd: Yag laser, a timer box and a data acquisition computer running Dynamic Studio software used for data acquisition and data processing.

Two Flow Sense cameras are positioned underneath the water channel at two different positions for data acquisition. After the accomplishment of the experimental cases for one location, cameras are shifted to the second location in order to observe the upper and lower regions of the flow structure. Figure 2.17 shows the two different camera arrangements and montage view of experimental setup for a certain position and angle of the tail.



a) 1st Camera Position



b) 2nd Camera Position

Figure 2.17 : Experimental Arrangement for Two Different Camera Locations.

After experimental setup is fully prepared, 25 gr silver coated hollow glass particles stated in the seeding section is added to the water to see the flow path more clear (while water is circulating in the channel).

During the experiment 3 different computers are used. 2 of the computers are responsible for the plunge motion of the wing. One of them controls the function of

the signal, amplitude and frequency of the motion via Labview Program, the other one controls the servo motor voltage. The third computer is responsible for data acquisition. It stores all PIV images on its hard drive.

To start the experiment, after the arrangement of the laser and control unit, data acquisition computer is set for acquisition (number of images time between pulses and trigger rate are entered) and then it started to wait for timer box's start signal.

After that, amplitude, frequency and function are inserted to the one of the other computers. Then, sub parameters (k_p and k_v) which are used for determining the precision and smoothness of the plunge motion are inserted to the third computer.

With the start signal, plunge motion is started. After the waiting for 20 seconds for making sure that starting effects are eliminated, laser is started to pulse and cameras are started data acquisition. Then stored data is saved in the data acquisition computer's database. These processes are repeated for all different cases and 73 sets of data are taken successfully. The detailed parameters of each set are given in Appendix A.1.

2.5.2 Post Processing

After the accomplishment of the experiments, images taken from different cameras at the same time should be stitched before the main data processing steps. Calibration data are used in order to stitch the all images as accurate as possible. Image stitching process is accomplished by a MATLAB script prepared by Dantec Dynamics Corporation and modified by Trisonic Laboratory's researchers. After inserting the pixel coordinates of two points showing the same thing in each image and inserting the scale factors of them; the MATLAB script resizes, rotates, translates and eventually stitches two separate images. Figure 2.18 represents any of two DPIV images before and after the stitching process.

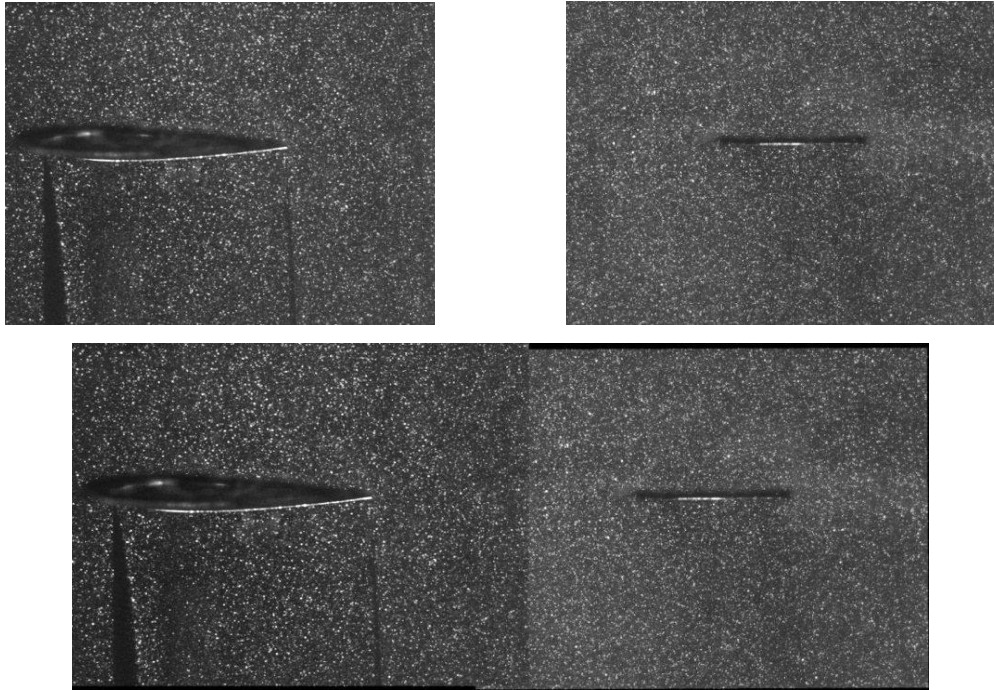


Figure 2.18 : Sample DPIV Image Before and After the Stitching Process.

It can be seen from the Figure 2.18 that stitching losses (seen at right top and left bottom of the stitched image) are so small as a result of good calibration process.

Figure 2.19 represents the field of view of the stitched images for the same experiment observed at two different locations.

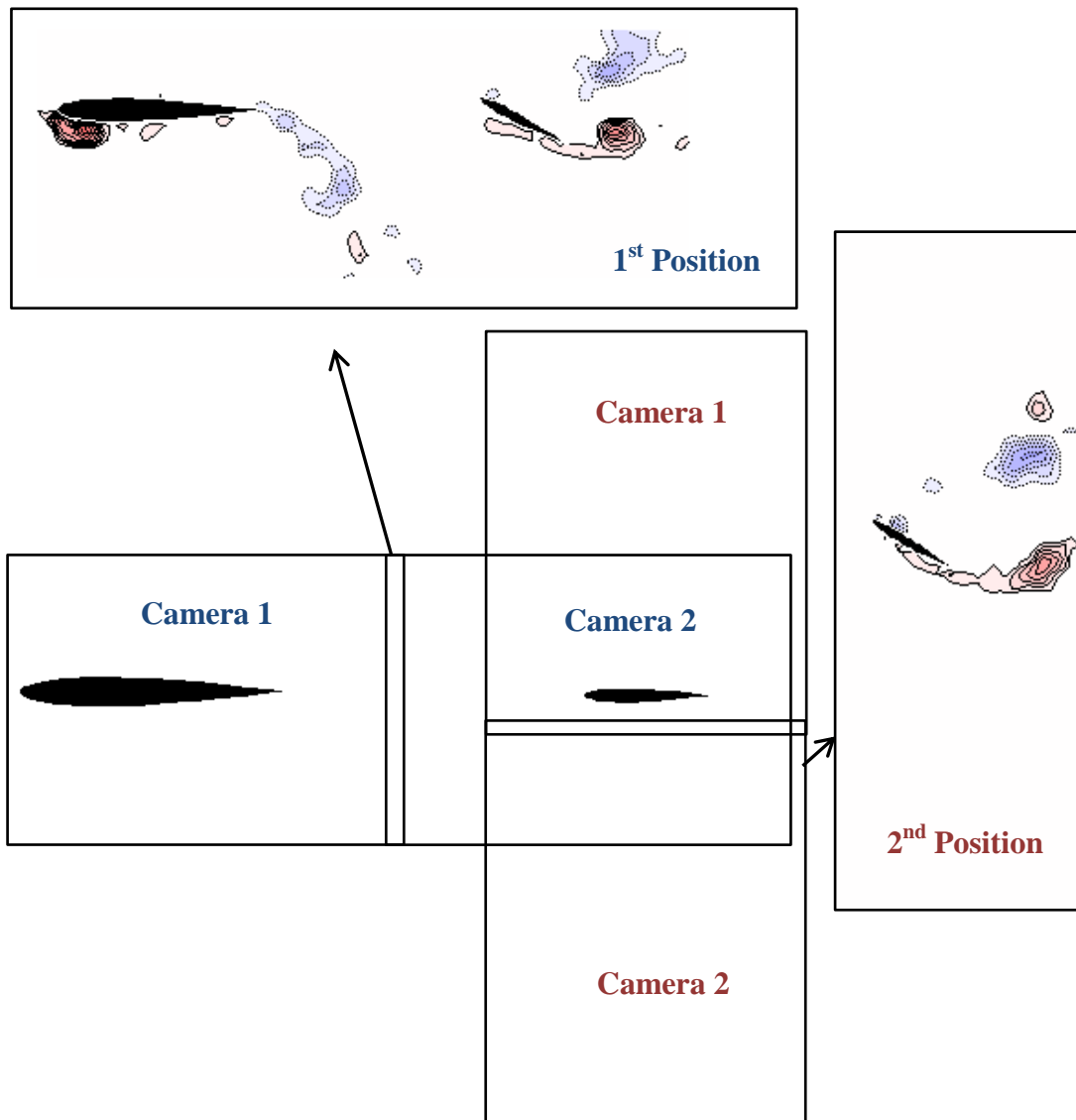


Figure 2.19 : Field of View of the Cameras for Two Different Positions.

Image properties after the both kind of stitching process are listed in Table 2.3.

Table 2.3 : Image Properties After the Stitching Process.

Settlement	Size of the Image (mm)	Vector Number
1 st Position	133.7 x 342.8	96 x 37 = 3552
2 nd Position	345 x 134.6	36 x 96 = 3456

The stitched images are interrogated using a double frame, cross-correlation technique with a window size of 64×64 pixels and 50% overlapping in each direction in order to determine the displacement vectors. Table 2.3 also shows the number of vectors belonging to the vector map of the each stitching process.

After the stitching process, plunging wing and the tail/flat plate are masked via MATLAB script couple created with the modification of a house written MATLAB script generated by Perçin at 2009. This script couple masks the plunging wing and the tail/flat plate for each stitched images. Although the location of the tail/flat plate does not changes from image to image for the same data set, the location of the plunging wing is differs from capture to capture. The script couple calculates the position of the plunging wing for each image and masks it according to the data acquisition and plunging parameters. Additionally, the code couple is also used for calculating the tail's position and angle. Therefore it can be used for all data sets independently. After accomplishment of the masking process, another house-written code NFILVB (Lin, 1994) is used for blanking out the vectors in the masked area.

After cancellation of the vectors being at the masking field, rest of the incorrect or bad vectors are eliminated by CleanVec program which is a house written DPIV vector validation software. This program finds the inconsistent vectors and deletes them for more accurate experimental results using the range validation and magnitude difference validation. Figure 2.20 shows a sample representing the elimination of the bad vectors via CleanVec program.

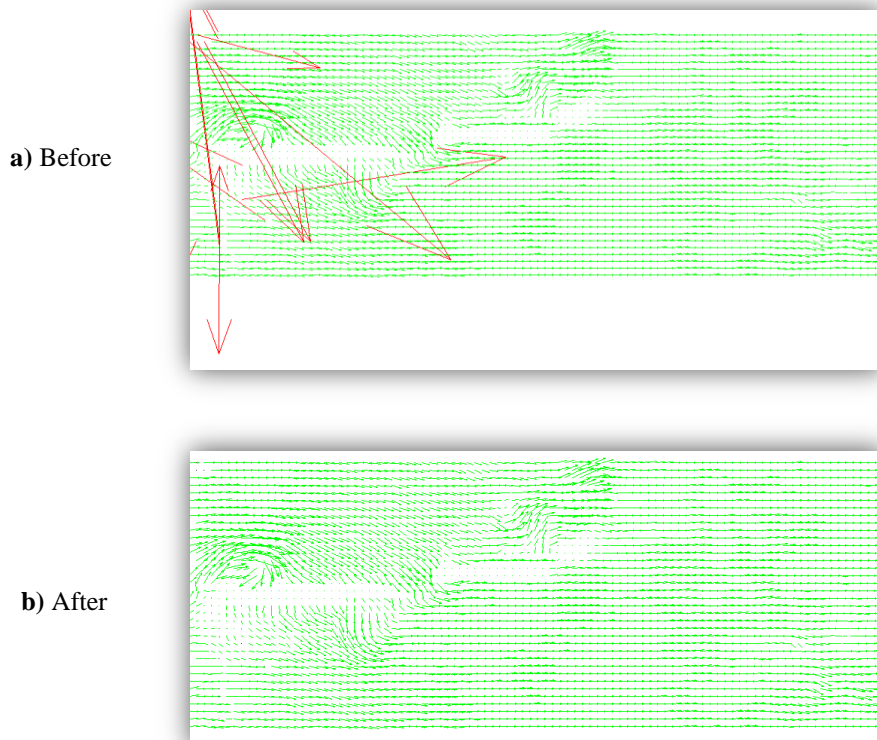


Figure 2.20 : Vector Cleaning Process.

After that, missing vectors are interpolated and filled with NFILVB program which is using a bi-linear least square fit technique on the surrounding vectors to fill the removed vector areas. Additionally, Gaussian weighted technique based on the Landreth and Adrian (1989) is also employed by the program for smoothing the resultant velocity field. In this study, 1.3 is used a suggested smoothing parameter.

Finally, the vector field with vorticity distribution is generated and another house-written program NWENSAW (Lin, 1996) is used in order to calculate the average vector magnitudes from the 200 images for each case. Then, results are displayed via Tecplot program.

3. RESULTS

Findings obtained from the processed results of the experiments are displayed and interpreted in this section. In order to find out the effects of tail location and tail angle on plunging wing's thrust/drag production several experiments have been conducted in the large scale water channel using Digital Particle Image Velocimetry (DPIV). Experiments are carried out for different non-dimensional plunge amplitudes (h), plunging frequencies (f), Reynolds numbers, tail positions (d) and tail angles (α) which are summarized in the Table 3.1.

Table 3.1 : Summary of the Experimental Parameters.

Re	h	f (Hz)	d (cm)	α (deg)
5000	0.25	0.2	0	0, 15 and 30
			2.5	0, 15 and 30
			5	0, 15 and 30
			10	0, 15 and 30
	0.05	0.4	0	0, 15 and 30
			2.5	0, 15 and 30
			5	0, 15 and 30
			10	0, 15 and 30
10000	0.25	0.4	0	0, 15 and 30
			2.5	0, 15 and 30
			5	0, 15 and 30
			10	0, 15 and 30

The data acquisition parameters which are the frequencies, period durations, image acquisition rates (trigger rate), number images per period, and total image numbers are also shown in the Table 3.2 and the sinusoidal plunging motion generated by the signal generator is illustrated in Figure 3.1.

Table 3.2 : Data Acquisition Parameters.

f (Hz)	T (sec)	Trigger Rate (Hz)	Image/Period	During How Many Periods	Total Image Number
0,2	5	10	50	4	200
0,4	2,5	10	25	8	200

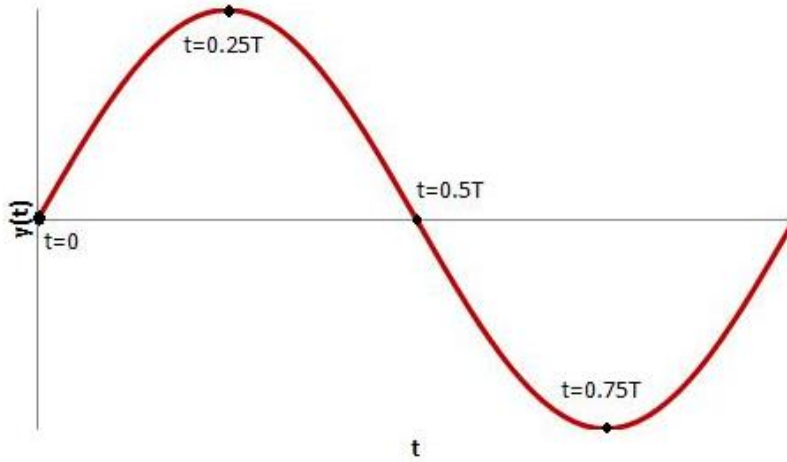


Figure 3.1 : Sinusoidal Motion of the Plunging Airfoil.

It is known from the previous studies that the sinusoidally plunging NACA 0012 airfoil (at $Re=5000$) produces thrust for $h=0.25$ and $f=0.2\text{Hz}$ ($k=1.25$). Additionally, the same motion of the same wing produces drag for $h=0.05$ and $f=0.4\text{Hz}$ ($k=2.5$) at the same Reynolds number. However it is further examined in this study that, whether it is possible to decrease the drag production or to increase the thrust with placing a NACA 0012 tail having the half-length chord of the plunging wing behind it using the vortical interactions or not. To investigate this, experiments are both conducted at $h=0.25$, $k=1.25$ and $h=0.05$, $k=2.5$ with placing the tail from the plunging wing at different distances and arranging it with different angles of attacks listed in the Table 3.1. Additionally, the result of doubling the plunging frequency and the Reynolds number is examined in this work. As a final effort, the NACA 0012 tail airfoil having 5 cm chord is replaced with a flat plate having the same length and the changes in the flow structure is investigated. 3 main results are obtained in consequence of experiments and each of them are examined in the following subsections.

3.1 Effects of Doubling the Plunging Frequency and Reynolds Number

For revealing the effect of doubling the plunging frequency and Reynolds number, experiments conducted at $h=0.25$, $Re=5000$, $f=0.2$ Hz for all different tail positions and angles are repeated for $h=0.25$, $Re=10000$, $f=0.4$ Hz by doubling the free-stream water velocity and plunging frequency. Since all experimental couples show the same attitude, only two experimental flow patterns are shown and their differences are interpreted.

Table 3.3 : Effects of Doubling the Reynolds Number and the Plunging Frequency for $d=5$ and $\alpha=30^\circ$.

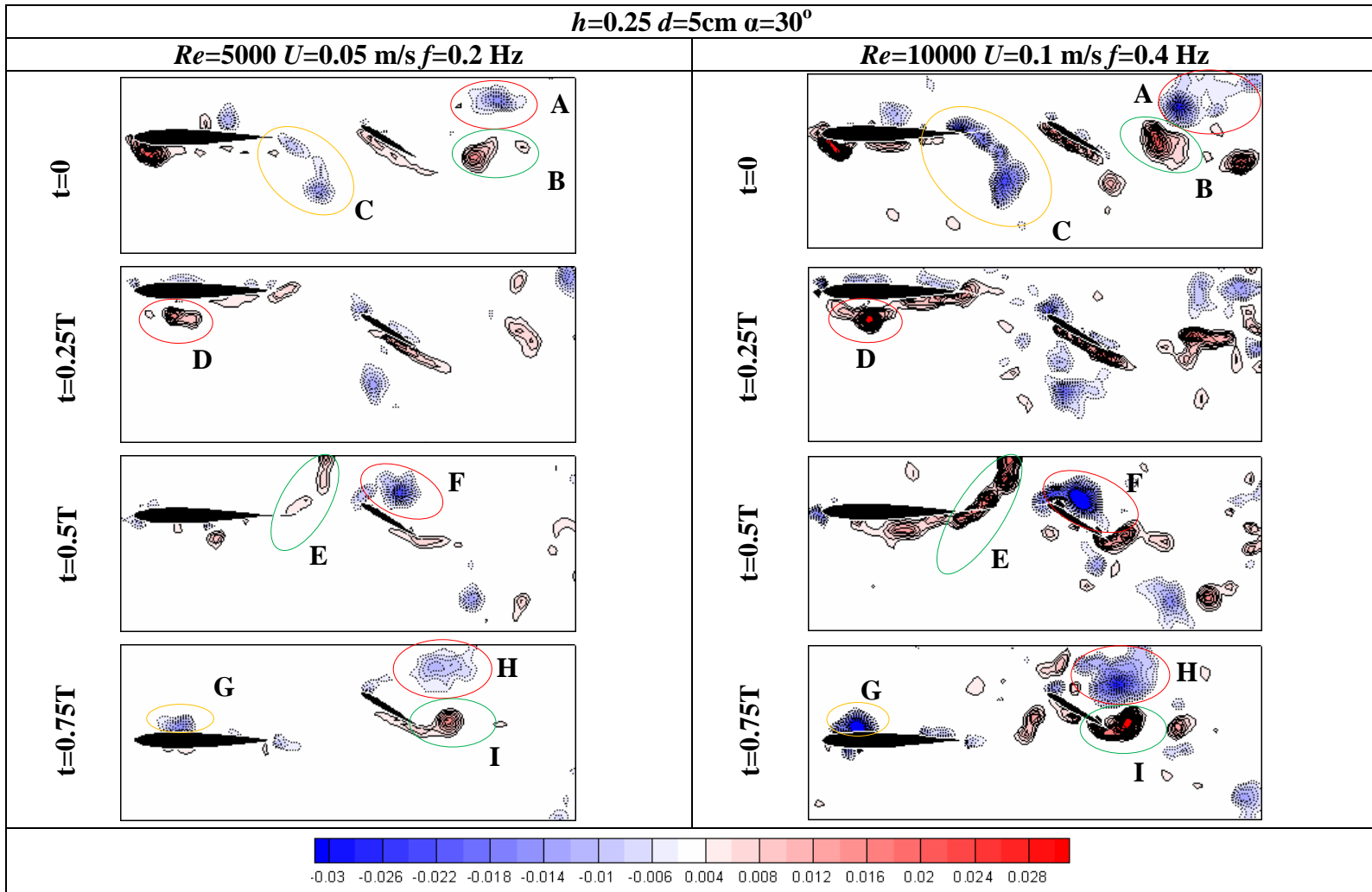
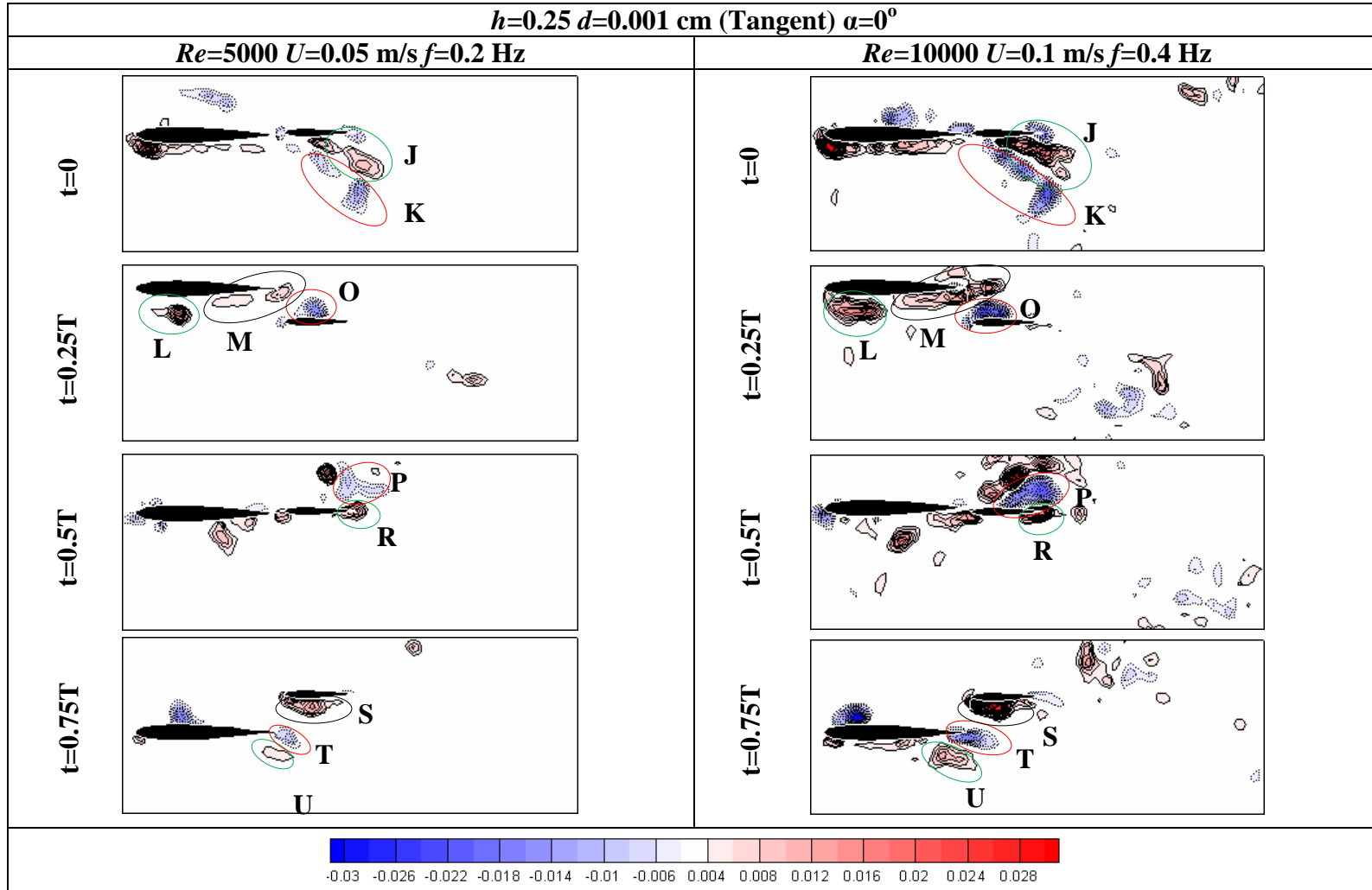


Table 3.4 : Effects of Doubling the Reynolds Number and the Plunging Frequency for $d=0$ and $\alpha=0^\circ$.



In Table 3.3 and 3.4 four instantaneous images per experimental case is represented in a column. Although 200 images are taken during the data acquisition process for each case, one period of a case can be represented by these four instantaneous images taken at $t=0$, $t=0.25T$, $t=0.50T$ and $t=0.75T$ due to the plunging motion is sinusoidal.

It can be obviously seen from the Table 3.3 and 3.4 that increment of the Reynolds number and plunging frequency results in the increment of the strength of the vortices without changing their places. This situation can be seen from the vortices tagged with letters from the foregoing figures. As a result, the flow structure does not change with doubling the both Reynolds number and plunging frequency; instead, existing vortex structure strengthens.

3.2 Investigation of the Best Tail Position and Orientation for Drag Minimization and Thrust Maximization

In this section, various tail positions and orientations are examined experimentally in order to find out whether it is possible to make drag minimization or thrust maximization with placing the tail airfoil behind the plunging wing using the vortical interactions or not. To reveal this, experimental measurements are taken at 4 different distances (d) and 3 different angles of attack where d is the distance between the trailing edge of the plunging airfoil and the leading edge of the tail airfoil. These distances and angles are listed in Table 3.1.

Table 3.5 to Table 3.10 represent the variation of the vortex structure with two different non-dimensional plunge amplitudes ($h=0.25$ and $h=0.25$) and corresponding plunging frequencies, for 4 different tail positions and 3 different angles of attack. All of the experimental results are represented by four instantaneous images which corresponds the only one period of airfoil's motion as it was in the previous section. Vortex sheds colored in red show the vortices rotating in the direction of counter clockwise and the blue ones show the vortices rotating in the direction of clockwise.

Table 3.5 : Instantaneous Vorticity Patterns for Different Tail Positions and Orientations-1.

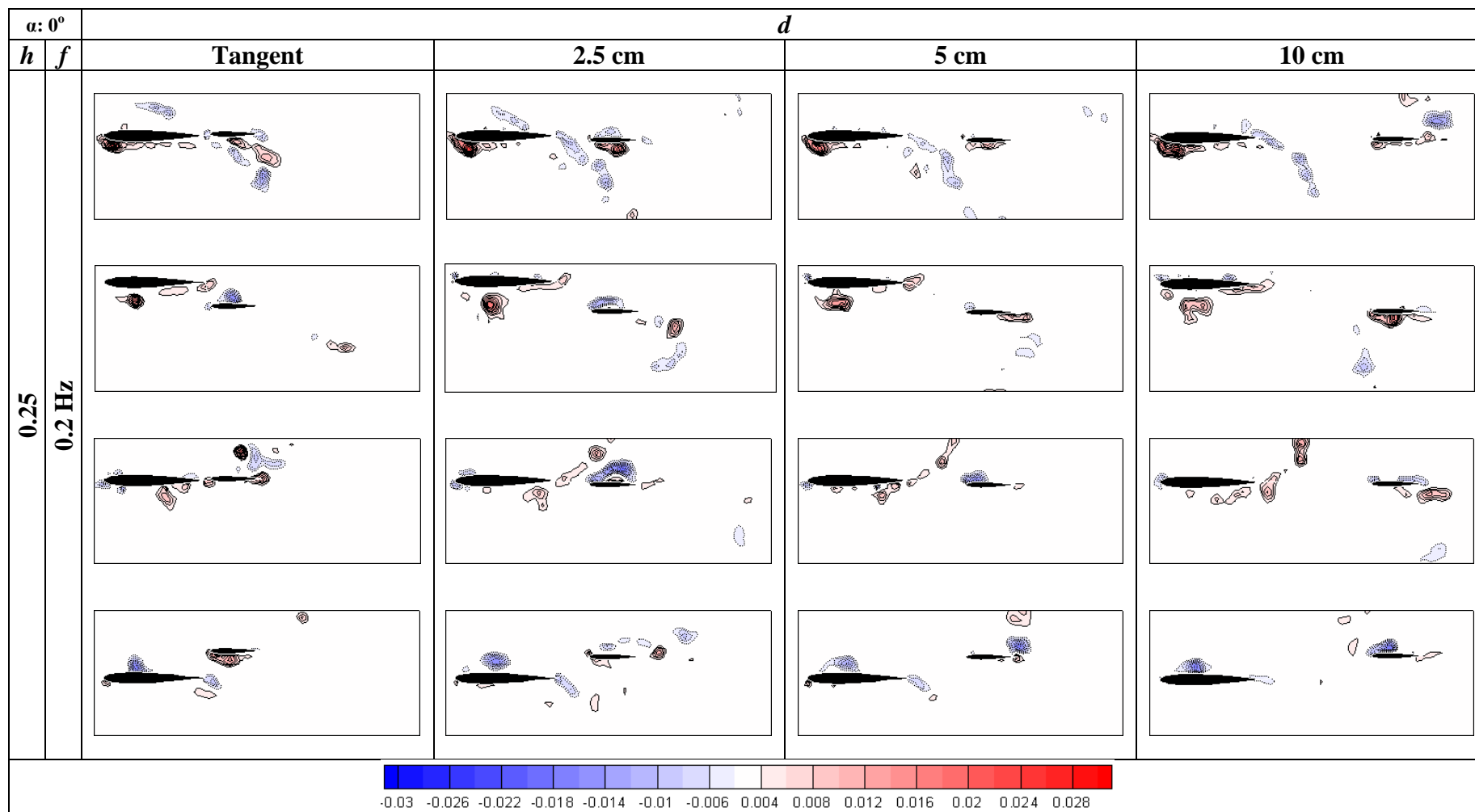


Table 3.6 : Instantaneous Vorticity Patterns for Different Tail Positions and Orientations-2.

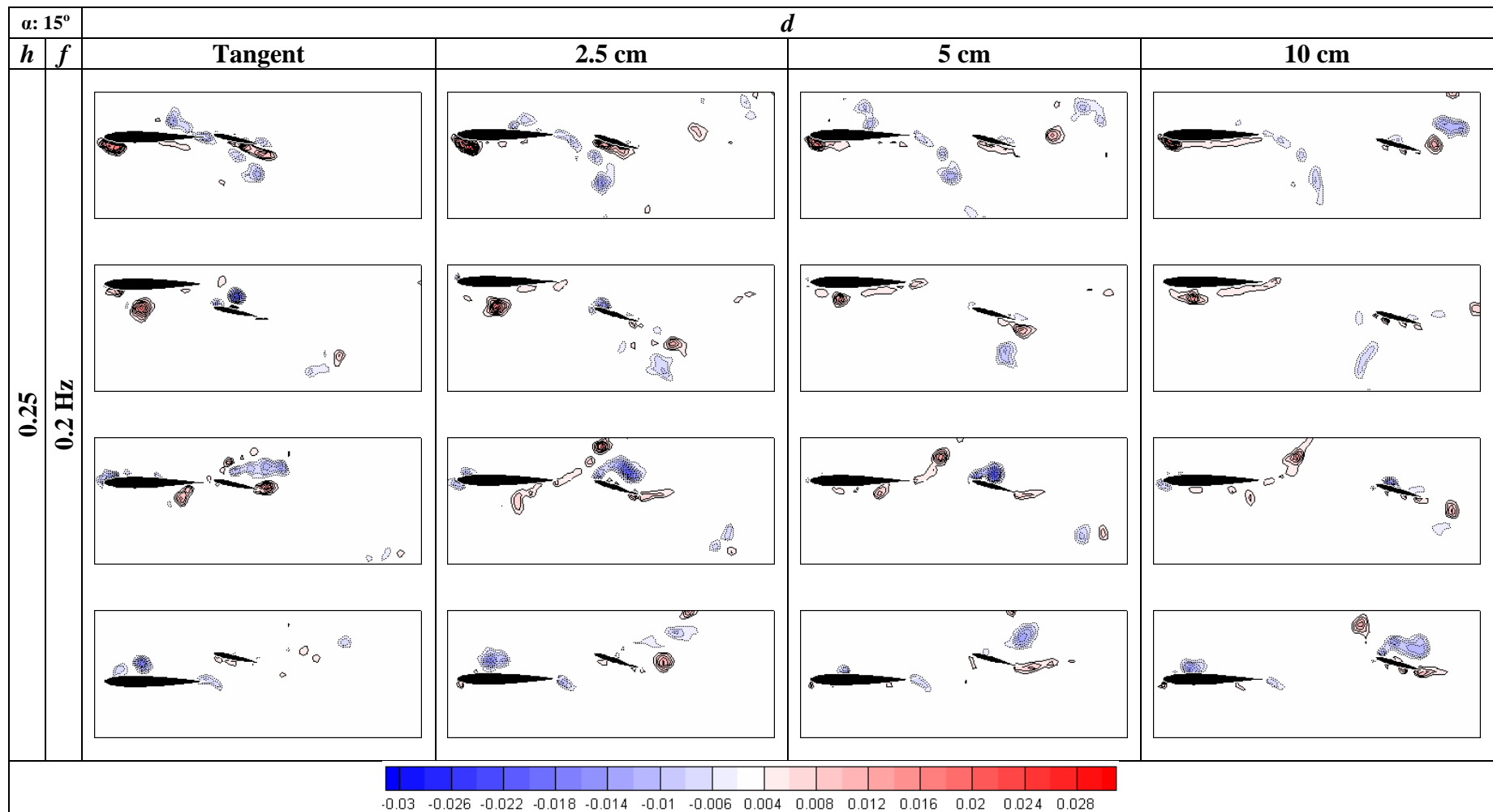


Table 3.7 : Instantaneous Vorticity Patterns for Different Tail Positions and Orientations-3.

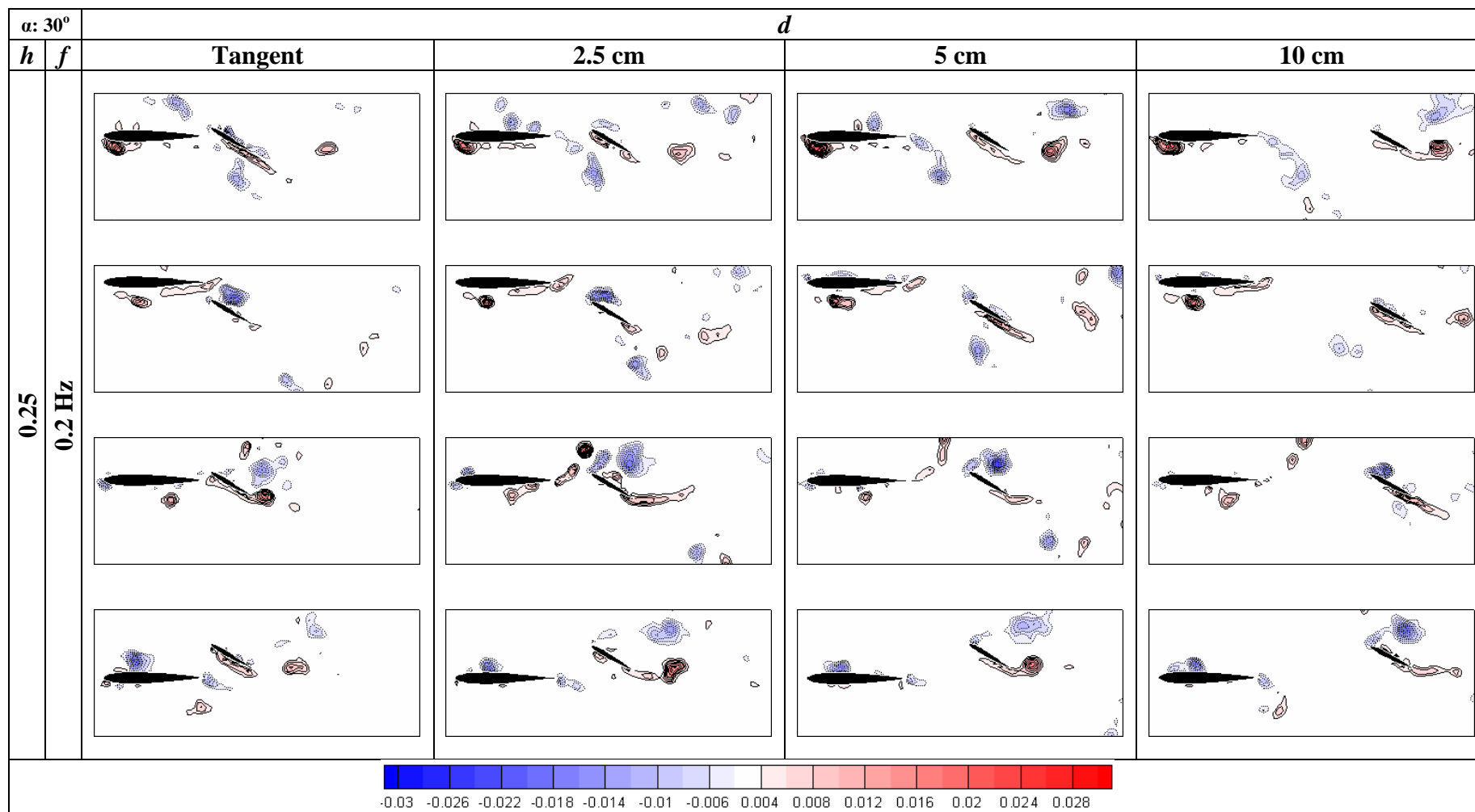


Table 3.8 : Instantaneous Vorticity Patterns for Different Tail Positions and Orientations-4.

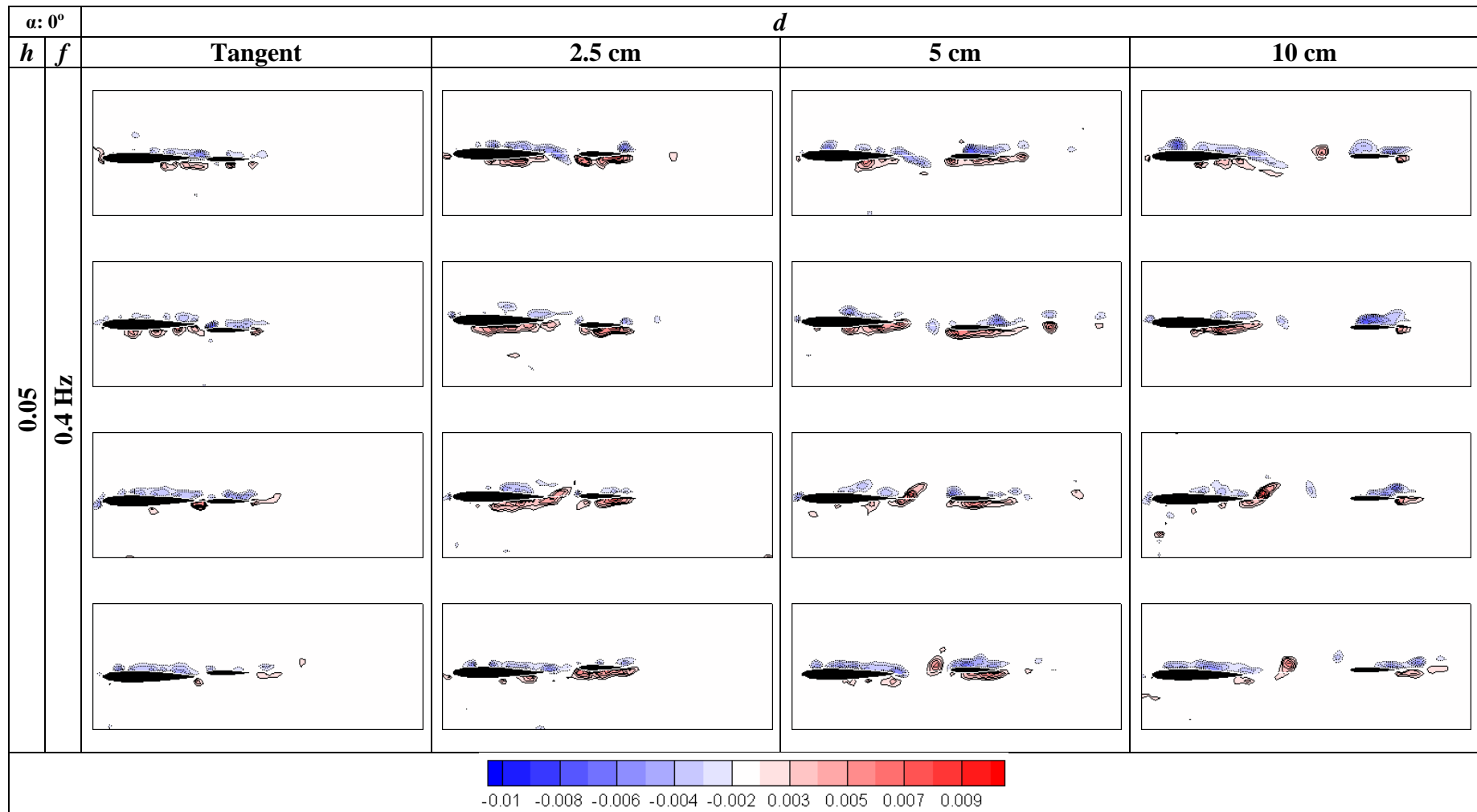


Table 3.9 : Instantaneous Vorticity Patterns for Different Tail Positions and Orientations-5.

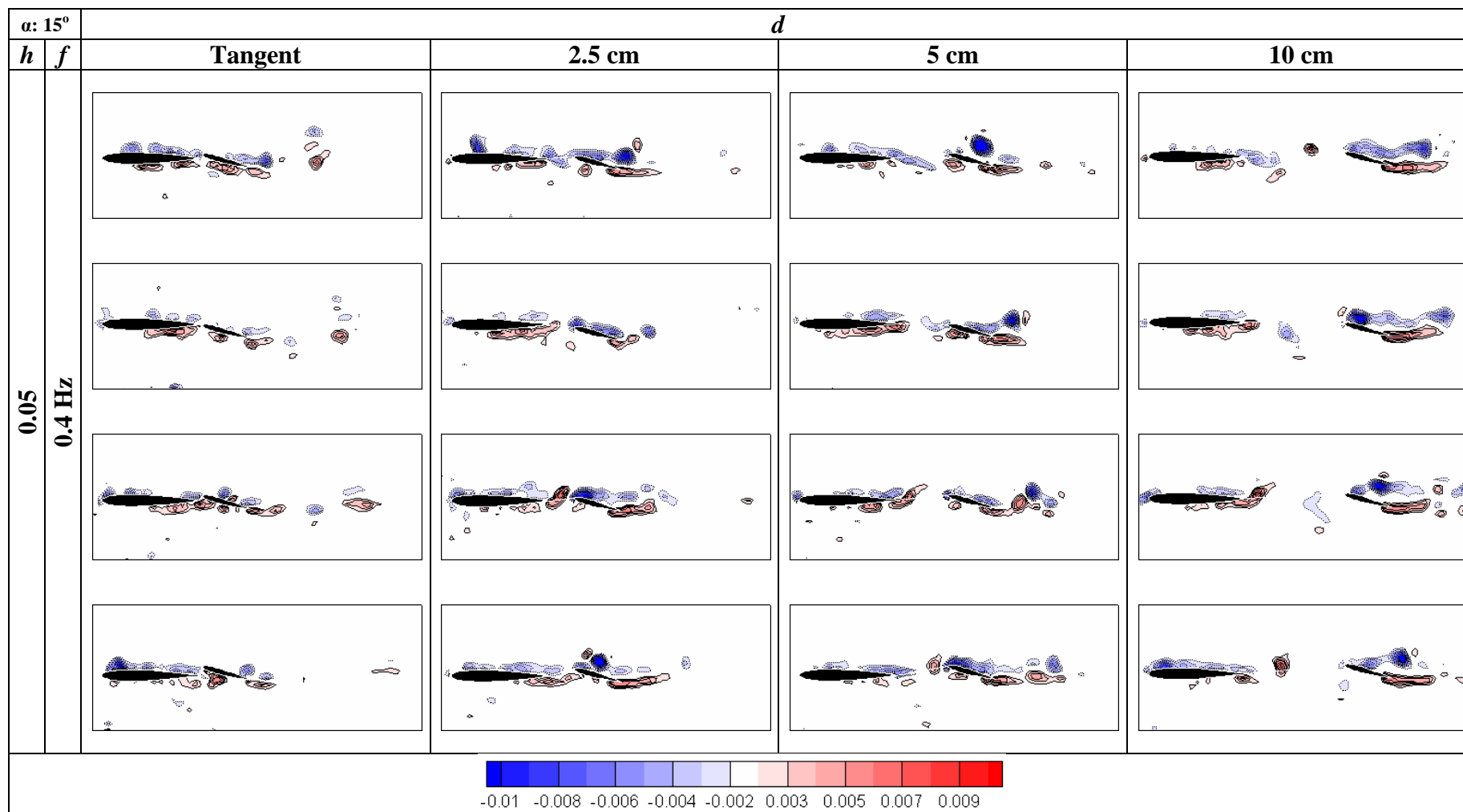
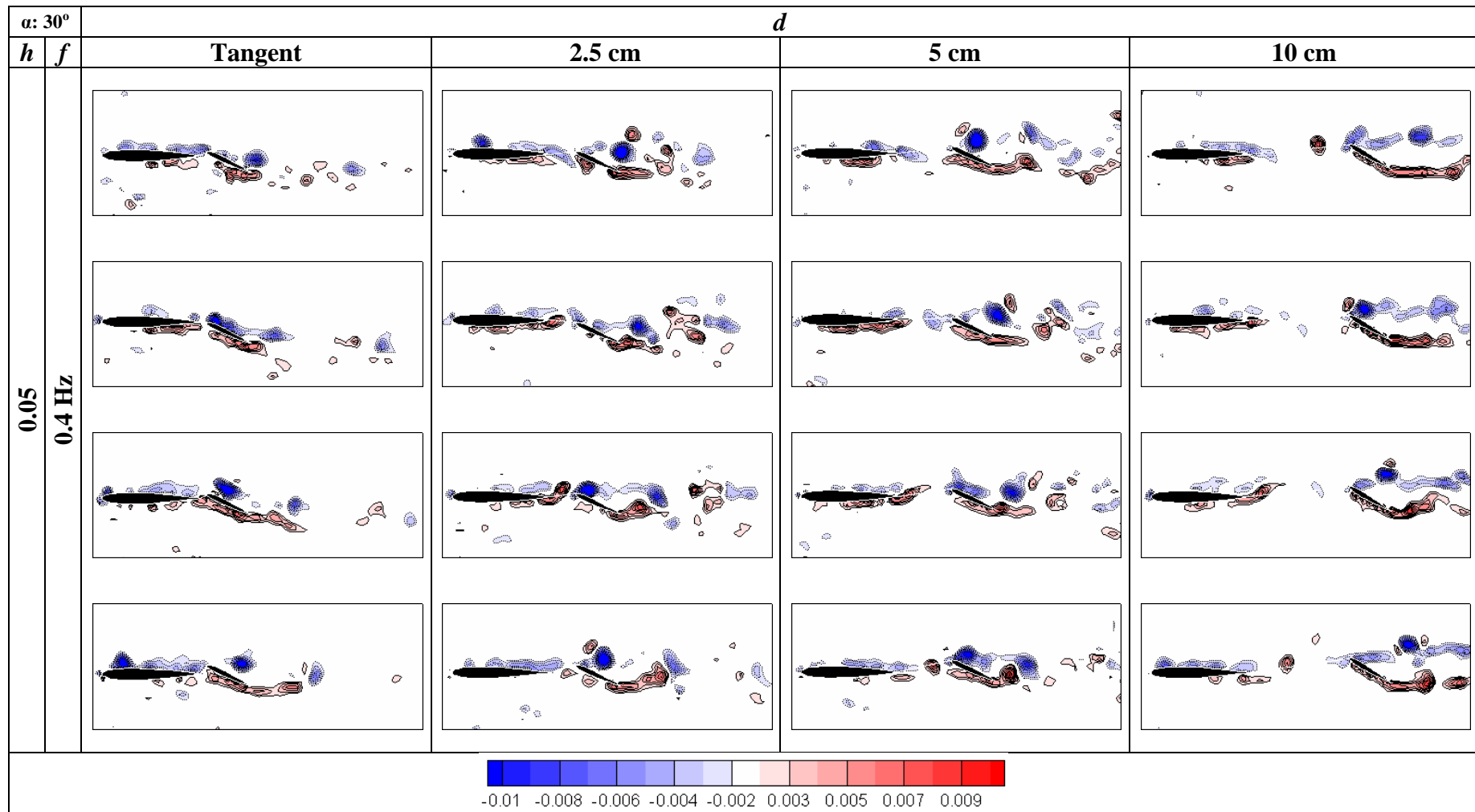


Table 3.10 : Instantaneous Vorticity Patterns for Different Tail Positions and Orientations-6.



It can be seen from the Table 3.6 to 3.10 that, when the distance between the plunging airfoil's trailing edge and the tail airfoil's leading is decreased; the tail starts to change the direction of the vortices by crossing their paths. This causes the alteration of the amount thrust or drag.

The drag production can be recognized by watching the turning directions of the vortices. If the vortex structure is like Karman Vortex Street; drag force is produced. This occurs when researcher see the blue vortex sheds upside the red ones. The reverse is also true for thrust producing cases. However, generally interpretations are made according to the average of the all instantaneous images, since the vortex sheds observed in one instantaneous image represents the situation for a very small time interval. In order to make a comparison between the different angles of attack, it can be stated that, increasing the angle of the tail strengthens the vortices which are obviously producing drag force. On the other hand, the change of the drag / thrust production depending on the position of the tail can be found out by examining the vectors just behind 5 cm (1 tail chord) of the tail airfoil. To accomplish this, camera positions are changed to the 2nd position shown in the Figure 2.19. Finally, the average velocity profiles just behind 5 cm of the tail airfoil for each experiment are determined and the free stream velocity is subtracted from these vectors for observing the momentum deficit or the jet like profile easily.

Table 3.11 to 3.13 shows the average velocity profiles for different tail positions and orientations. While making this tabulation two different colors are used in order to classify the magnitudes of the velocity profiles. The vectors shown with blue are magnified two times according to the red vectors. Without making this adjustment, it is very difficult to see the differences of experimental results conducted for 0 degree tail angle. As a result, velocity profiles having the same color can easily compared among them.

Table 3.14 to 3.16 also shows the average resultant velocity profiles for different tail positions and orientations.

Table 3.11 : Averaged Velocity Profiles ($U-U_\infty$) for Different Tail Positions and Orientations-1.

			d			
h	f	α	Tangent	2.5 cm	5 cm	10 cm
0.25	0.2 Hz	0°				
		15°				

Table 3.12 : Averaged Velocity Profiles ($U-U_\infty$) for Different Tail Positions and Orientations-2.

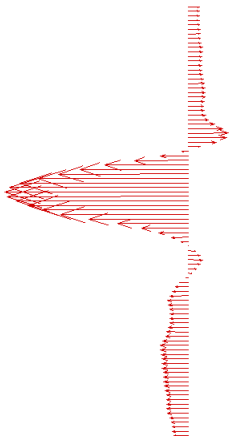
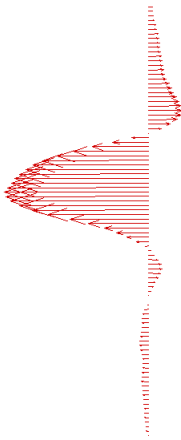
			<i>d</i>			
<i>h</i>	<i>f</i>	α	Tangent	2.5 cm	5 cm	10 cm
0.25	0.2 Hz	30°				
0.05	0.4 Hz	0°				

Table 3.13 : Averaged Velocity Profiles ($U-U_\infty$) for Different Tail Positions and Orientations-3.

			d			
h	f	α	Tangent	2.5 cm	5 cm	10 cm
0.05	0.4 Hz	15°				
		30°				

Table 3.14 : Averaged Resultant Velocity Profiles (U) for Different Tail Positions and Orientations-1.

			d			
h	f	α	Tangent	2.5 cm	5 cm	10 cm
0.25	0.2 Hz	0°				
		15°				

Table 3.15 : Averaged Resultant Velocity Profiles (U) for Different Tail Positions and Orientations-2.

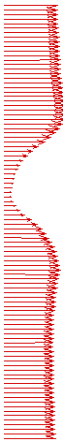
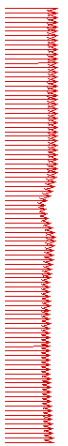
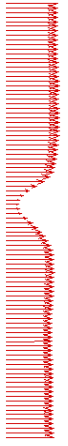
			d			
h	f	α	Tangent	2.5 cm	5 cm	10 cm
0.25	0.2 Hz	30°				
0.05	0.4 Hz	0°				

Table 3.16 : Averaged Resultant Velocity Profiles (U) for Different Tail Positions and Orientations-3.

			d			
h	f	α	Tangent	2.5 cm	5 cm	10 cm
0.05	0.4 Hz	15°				
		30°				

According to the tables above, while wing is plunging with the parameters of $h=0.25$ and $f=0.2\text{Hz}$, any increment in tail airfoil's angle of attack results in the increment of the total drag force as expected and the same situation is also valid for the plunging wing with parameters of $h=0.05$ and $f=0.4\text{Hz}$. Additionally, from the foregoing tables it is trivial that there is a drag reduction between the $d=2.5\text{cm}$ distance to the tangent position (nearly $d=0\text{ cm}$) for all cases. This is mainly arises from the chopping effect which occurs since tail airfoil crosses the vortex paths and direct them to another position.

For making further interpretations, it is suitable to sum up the vectors (shown at Table-11, Table-12 and Table-13) in a line by assuming that every vector represents the average value of vectors throughout 3.54 mm distance. Therefore, the 96 vectors in line shown in the tables above can summed up and, gathered value is used for interpreting the results. The left side of the vectors is taken as the positive (+) direction while right side is negative (-) for easily observing the increment and decrement in the drag production throughout the four different tail positions.

The following graphs give valuable information about the magnitude of the thrust/drag force production of the system at a specific angle of attack for different tail positions. The graph shown in Figure 3.2 is plotted only for the plunging wing parameters of $h=0.25$ and $f=0.2\text{ Hz}$.

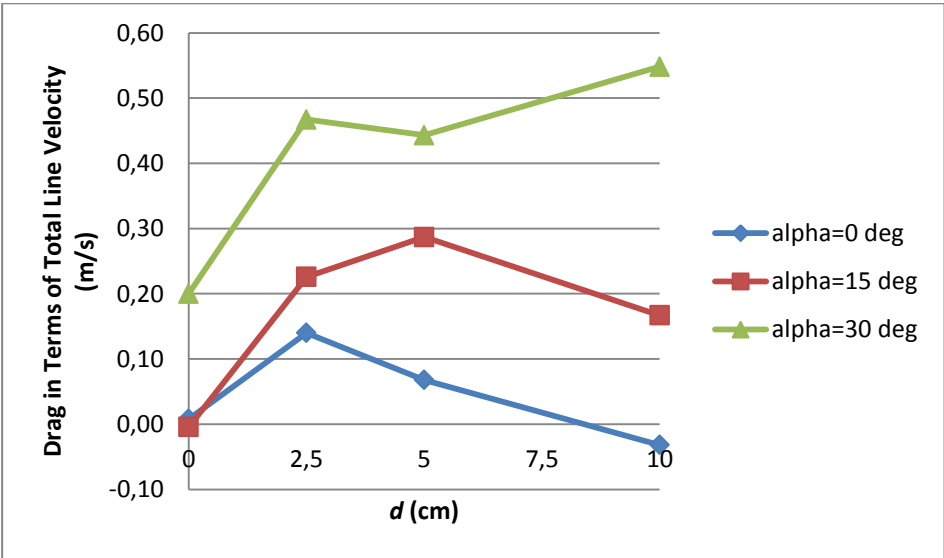


Figure 3.2 : Variation of Thrust/Drag Production Depending on Position and Orientation of the Tail for $h=0.25$ and $f=0.2\text{ Hz}$.

If the experiments shown in the Figure 3.2 is done with the same parameters without placing the tail, there will be seen a thrust production. However, placing a tail behind the plunging wing causes not only the reduction of thrust but also the increment of drag. Only the case where $\alpha=0$ degree and $d=10$ cm continues to produce thrust. Reducing the distance d from 10 cm to 2.5 cm results in the increment of the drag production. On the other hand, when the tail is located just behind the airfoil as tangent (nearly $d=0$) the amount of produced drag decreases drastically due to the chopping effect.

The graph shown in Figure 3.3 is plotted only for the plunging wing parameters of $h=0.05$ and $f=0.4$ Hz. If the experiments are conducted with the same parameters without placing the tail behind the plunging wing, there will be seen a drag production.

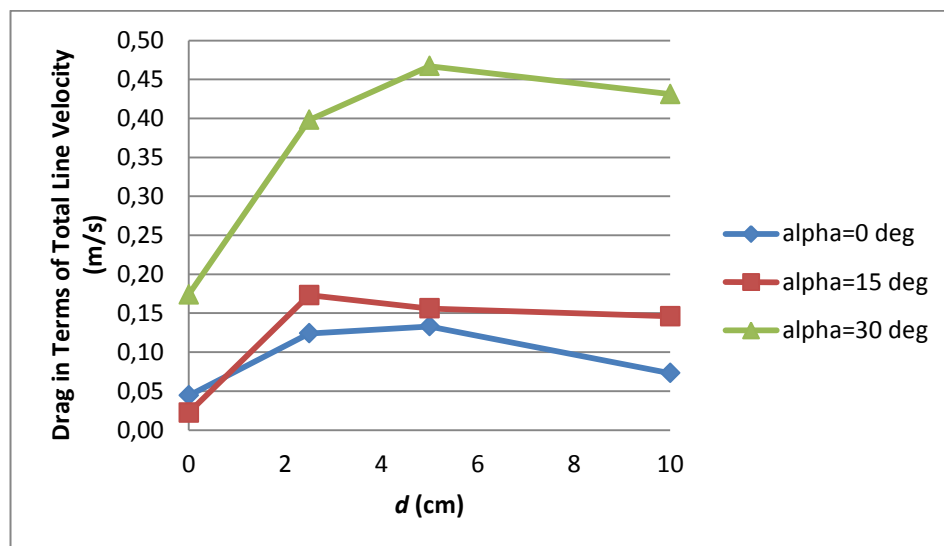


Figure 3.3 : Variation of Thrust/Drag Production Depending on Position and Orientation of the Tail for $h=0.05$ and $f=0.4$ Hz.

In this situation placing a tail behind the plunging wing causes the increment of the present drag. While the drag production is a bit less at relatively far places like $d=10$ cm, it increases with the approximation of the tail to the plunging wing up to nearly $d=2.5$ cm distance. After that position any movement of the tail towards the plunging wing results in the reduction of the drag as it was observed in the previous cases.

Examining both of the Figure 3.2 and 3.3, it can be stated that, augmenting the angle of attack results in the increment of the drag production for all experimental cases and combining these two graphs Figure 3.4 can be generated.

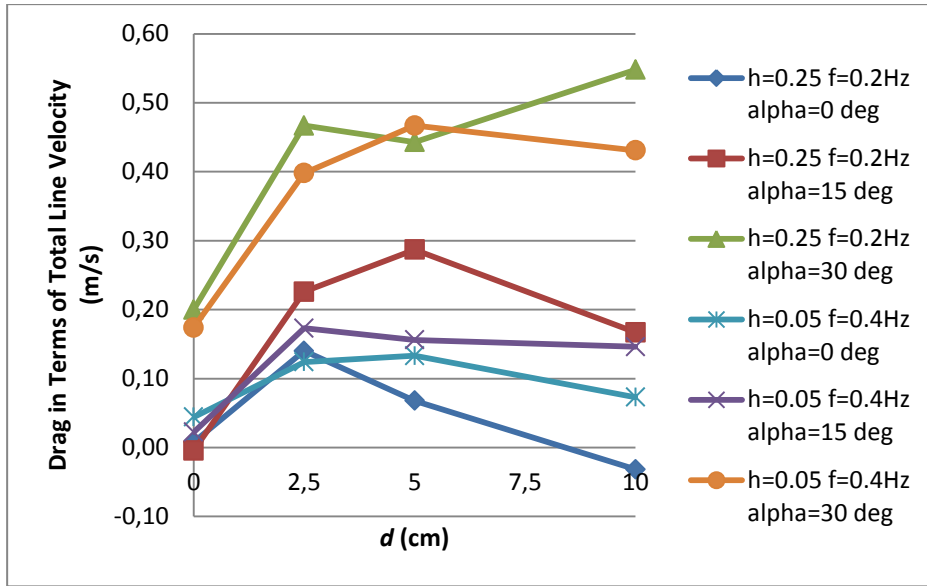


Figure 3.4 : Variation of Thrust/Drag Production Depending on Position and Orientation of the Tail for All Cases.

The drag production for the cases whose plunging parameters are: $h=0.25$ and $f=0.2$ Hz are more than the other experimental sets whose parameters are: $h=0.05$ and $f=0.4$ Hz for $\alpha=15^\circ$ and $\alpha=30^\circ$.

3.3 Effects of Changing the Tail Airfoil with a Flat Plate

For determining the effects of replacing the NACA 0012 airfoil having 5 cm chord with a flat plate having same length, the experiments conducted at $h=0.25$, $Re=5000$ and 10000 , $f=0.2$ Hz and 0.4 Hz for all different tail positions and for only 0 degree angle of attack are repeated by replacing the tail airfoil with a flat plate having a thickness of 1.5 mm and a length of 5 cm.

Table 3.17 and 3.18 is generated for making a comparison between the effects of airfoil and flat plate on the flow structure. Since all experimental couples show the same attitude, only two experimental flow patterns are shown and their differences are interpreted as it was in the Section 3.1.

It can be obviously seen from the Table 3.17 and 3.18 that flow structure presents almost the same behavior when the tail airfoil is replaced by a thin flat plate having the same chord length. This event can be observed from the vortices tagged with letters from the images shown in the tables below. The source of negligibly small differences on the flow structure between two different types of tails is airfoil's sharp trailing edge.

Table 3.17 : Effects of Replacing the Tail Airfoil with a Flat Plate for $Re=10000$ and $d=0$.

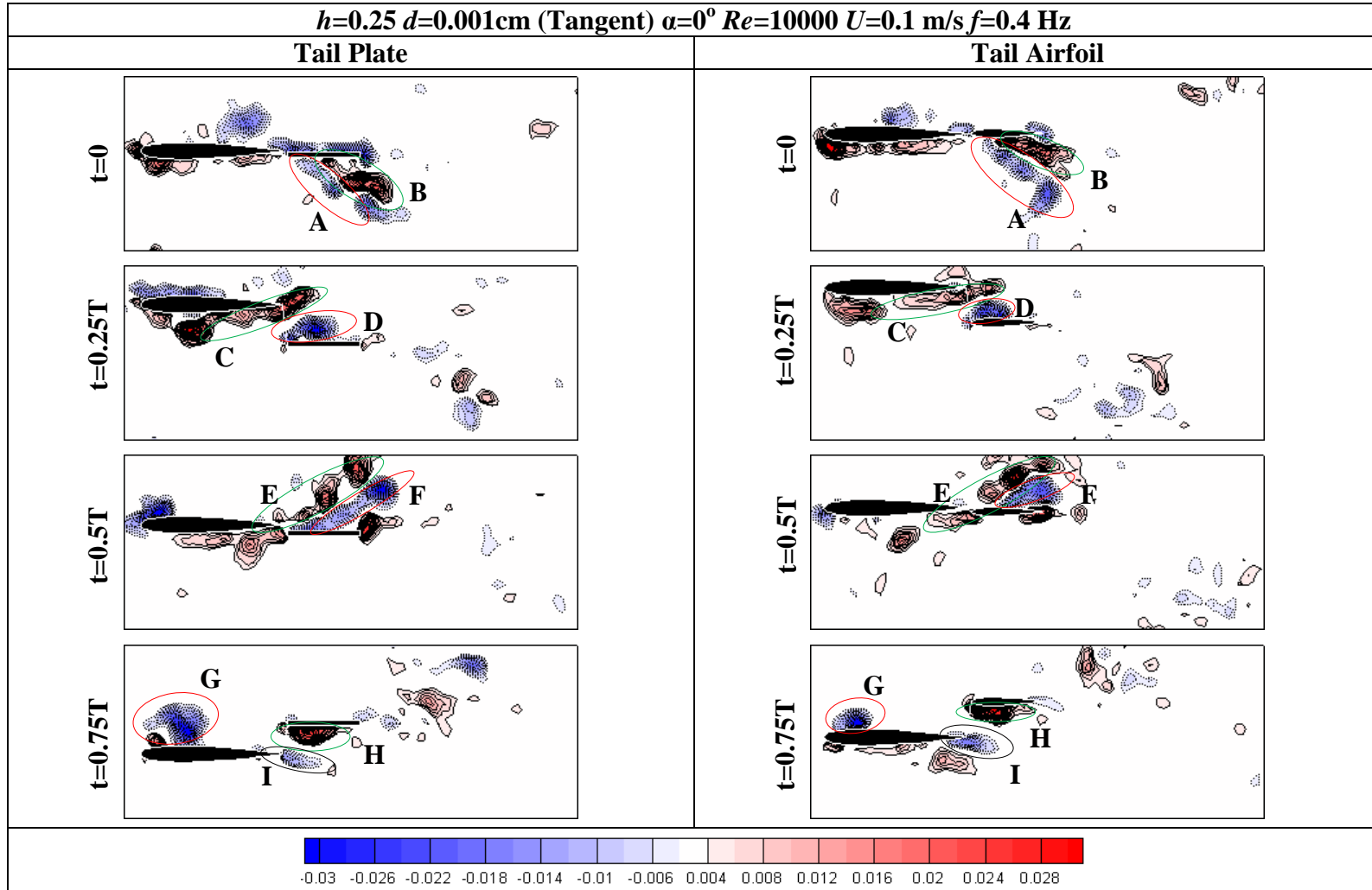
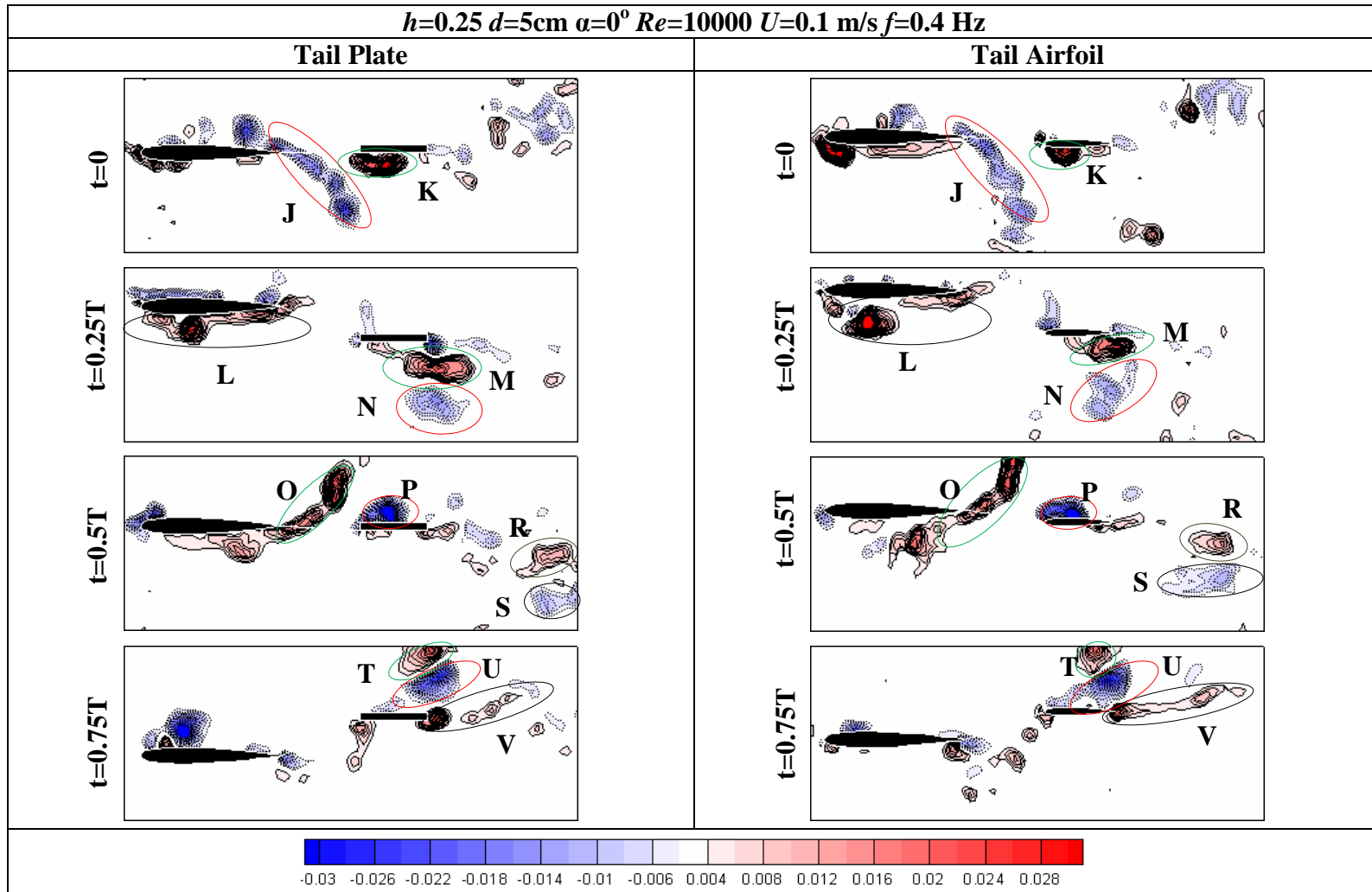


Table 3.18 : Effects of Replacing the Tail Airfoil with a Flat Plate for $Re=10000$ and $d=5$ cm.



4. CONCLUSION

In this experimental study, the possibility of decreasing drag or increasing thrust production via vortical interactions due to presence of a tail airfoil behind a plunging wing is investigated using Digital Particle Image Velocimetry (DPIV) Method in order to assist the development of new generation, more efficient Micro Air Vehicles. Additionally, the effect of doubling the plunging frequency and the Reynolds number on flow structure is also examined within the scope of this work. As a final effort, the effect of replacing the tail airfoil with a flat plate (having same length with the tail airfoil's chord) on flow structure (only for 0 deg angle of attack) is investigated.

Results of the experiments revealed that when the tail airfoil is close enough to the plunging wing, it starts to change the direction of vortices shedding from the plunging wing by crossing their paths. This causes the alteration of the amount thrust or drag. However, instead of thrust production reduction of drag is observed especially for closely placed tail airfoil at a horizontal distance of 2.5 cm to the trailing end of the plunging wing for all experimental cases. This can be called as chopping effect. Additionally, any increase in the tail airfoil's angle of attack resulted in an increase of wake deficit, i.e. the total drag force acting on the airfoil couple, as it was predicted.

According to the results of the second set of experiments, the flow structure does not change with doubling both Reynolds number and plunging frequency; instead, existing vortex structure strengthens. In other words, flapping the wing at higher frequencies and increasing the free stream velocity strengthens the vortices, but does not change their location arrangement. Additionally, the flow structure exhibits virtually the same development when the tail airfoil is replaced with a thin flat plate having the same chord length. Negligibly small differences in the flow structures for two different types of tail geometry arise due to the difference of the leading edge geometry.

As a result, drag is not converted to the thrust by placing a tail behind a plunging wing; but, drag reduction is obtained by placing a tail airfoil just behind the oscillating airfoil. Therefore, it may be possible to convert the drag to small amount of thrust for a certain set of experimental parameters. Disclosing this issue requires further experiments by also using different airfoil profiles.

5. REFERENCES

- Ames, R., Wong, O., and Komerath, N., 2001: On the Flowfield and Forces Generated by a Flapping Rectangular Wing at Low Reynolds Number, *Fixed and Flapping Wing Aerodynamics for Micro Air Vehicle Applications*.
- Andersen, N. A., 2007: Camera Technology and Advanced Imaging Applications, Dantec Dynamics.
- Anderson, J. M., Streitlien, K., Barrett, D. S., and Triantafyllou, M. S., 1998: Oscillating Foils of High Propulsive Efficiency, *Journal of Fluid Mechanics*, Vol. **360**, pp. 41-72.
- Ansari, S. A., Zbikowski, R., and Knowles, K., 2006: Non-linear Unsteady Aerodynamic Model for Insect-Like Flapping Wings in the Hover. Part 2: Implementation and Validation, *Journal of Aerospace Engineering*, Vol. **220**, Part G:J.
- Antonnen, J. S. R., King, P. I., and Beran, P. S. 2005: Applications of Multi-POD to a Pitching and Plunging Airfoil, *Mathematical and Computer Modelling*, Vol. **42**, pp. 245-259.
- Betz, A., 1912: Ein Beitrag zur Erklärung des Segelfluges, *Zeitschrift für Flugtechnik und Motorluftschiffahrt*, Vol. **3**, pp. 269-272.
- Birch, D., and Lee, T., 2005: Investigation of the Near-Field Tip Vortex Behind and Oscillating Wing, , *Journal of Fluid Mechanics*, Vol. **544**, pp. 201-241.
- Blondeaux, P., Fornarelli, F., Guglielmini, L., Triantafyllou, M. S., and Verzicco, R., 2005: Numerical Experiments on Flapping Foils Mimicking Fish-Like Locomotion, *Physics of Fluids*, Vol. **17**.
- Bomphrey, R. J., 2006: Insects in Flight: Direct Visualization and Flow Measurements, *Institute of Physics Publishing – Bio Inspiration and Biomimetic*, pp. S1-S9.
- Brunton, S. L., Rowley, C. W., Taira, K., Colonius, T., Collins, J., and Williams, D. R., 2008: Unsteady Aerodynamic Forces on Small-Scale Wings: Experiments, Simulations and Models, *AIAA 2008-520 (Reno)*.
- Cetiner, O., 2010: PIV (Particle Image Velocimetry), Lecture Notes.
- Chandar, D. D. J., and Damodaran, M., 2008: Computational Study of Unsteady Low-Reynolds Number Airfoil Aerodynamics Using Moving Overlapping Meshes, *AIAA Journal*, Vol. **46**, No. 2, pp. 429-438.
- Fenercioglu, I., and Cetiner, O., 2008: Flow Structures Around an Oscillating Airfoil in Steady Current, *14th Symposium on Applications of Laser Techniques to Fluid Mechanics*, Lisbon.

- Freytmuth, P.**, 1988: Propulsive Vortical Signature of Plunging and Pitching Airfoils, *AIAA Journal*, Vol. **26**, No. 7.
- Fuchiwaki, M., and Tanaka, K.**, 2006: Vortex Structure and Scale on an Unsteady Airfoil, *Japan Society Mechanical Engineering International Journal*, Vol. **49**, No. 4, pp. 1056-1063.
- Garrick, I. E.**, 1936: Propulsion of a Flapping and Oscillating Airfoil, *NACA Report 567*.
- Guglielmini, L., and Blondeaux P.**, 2004: Propulsive Efficiency of Oscillating Foils, *European Journal of Mechanics B/Fluids*, Vol. **23**, pp. 255-278.
- Guvernyuk, S. V., and Dynnikova, G. Ya.**, 2006: Modeling the Flow past an Oscillating Airfoil by the Method of Viscous Vortex Domains, *Fluid Dynamics*, Vol. **42**, No. 1, pp. 3-14.
- Hamdani, H., and Sun, M.**, 2000: Aerodynamic Forces and Flow Structures of an Airfoil in Some Unsteady Motions at Small Reynolds Number, *Acta Mechanica*, Vol. **145**, pp. 173-187.
- Han, C., and Cho, J.**, 2006: Unsteady Aerodynamic Analysis of Flat Plates in Pitch Oscillation, *AIAA Journal*, Vol. **44**, No. 6, pp. 1121-1226.
- Han, C., Lee, H., and Cho, J.**, 2008: Propulsive Characteristics of Dual Fish-Like Foils, *Journal of Mechanical Science and Technology*, Vol. **22**, pp. 171-179.
- Heathcote, S., and Gursul I.**, 2007: Jet Switching Phenomenon for Periodically Plunging Airfoil, *Physics of Fluids*, Vol. **19**.
- Heathcote, S., Wang, Z., and Gursul, I.**, 2008: Effect of Spanwise Flexibility on Flapping Wing Propulsion, *Journal of Fluids and Structures*, Vol. **24**, pp. 183-189.
- Ho, Chin-Ming, and Chen**, 1980: Unsteady Wing of a Plunging Airfoil, *AIAA 80-1446 (Snowmass Colorado)*.
- Hong, Y. S., and Altman, A.**, 2007: Streamwise Vorticity in Simple Mechanical Flapping Wings, *Journal of Aircraft*, Vol. **44**, No. 5, pp. 1588-1597.
- Isaac, K. M., Rolwes, J. and Colozza, A.**, 2008: Aerodynamics of a Flapping and Pitching Wing Using Simulations and Experiments, *AIAA Journal*, Vol. **46**, No. 6, pp. 1505-1515.
- Jones, K. D., Dohring, C. M., and Platzer, M. F.**, 1996: Wake Structures Behind Plunging Airfoils: A Comparison of Numerical and Experimental Results, *AIAA 96-007(Reno)*.
- Jones, K. D., Dohring, C. M., and Platzer, M. F.**, 1998: Experimental and Computational Investigation of the Knoller-Betz Effect, *AIAA Journal*, Vol. **36**, No. 7.
- Jones, K. D., and Platzer, M. F.**, 1999: An Experimental and Numerical Investigation of Flapping-Wing Propulsion, *AIAA 99-0995 (Monterey)*.

- Jung, Y. W., and Park, S. O.,** 2005: Vortex-Shedding Characteristics in the Wake of an Oscillating Airfoil at Low Reynolds Number, *Journal of Fluids and Structures*, Vol. **20**, pp. 451-464.
- Katzmayr, R.,** 1922: Effect of Periodic Changes of Angle of Attack on Behavior of Airfoils, *NACA TM 147*.
- Kaya, M., and Tuncer, I. H.,** 2004: Üst Üste Çırpan İki Kanat Kesitinin Maksimum İtici İçin Paralel Eniyileştirilmesi, *5th Kayseri Aerospace Symposium*, Kayseri.
- Knoller, R.,** 1909: Die Gesetze des Luftwiderstandes, *Flug- und Motortechnik (Wien)*, Vol. **3**, No. 21, pp. 1-7.
- Koochesfahani, M. M.,** 1989: Vortical Patterns in the Wake of a Oscillating Airfoil, *AIAA Journal*, Vol. **27**, No. 9.
- Lai, J. C. S., and Platzer, M. F.,** 1999: Jet Characteristics of a Plunging Airfoil, *AIAA Journal*, Vol. **37**, No. 12.
- Lan, S. L., and Sun, M.,** 2001: Aerodynamic Force and Flow Structures of Two Airfoils in Flapping Motions, *Acta Mechanica*, Vol. **17**, No. 4, pp. 310-331.
- Lewin, G. C., and Haj-Hariri, H.,** 2003: Modelling Thrust Generation of a Two Dimensional Heaving Hydrofoil in a Viscous Flow, *Journal of Fluid Mechanics*, Vol. **492**, pp. 339-362.
- Lu, X. -Y., Yang, J. -M., and Yin, X. -Z.,** 2003: Propulsive Performance and Vortex Shedding of a Foil in Flapping Flight, *Acta Mechanica*, Vol. **165**, pp. 189-206.
- Lua, K. B., Lim, T. T., and Yeo, K. S.,** 2007a: Wake-Structure Formation of a Heaving Two-Dimensional Elliptic Airfoil, *AIAA Journal*, Vol. **45**, No. 7.
- Lua, K. B., Lim, T. T., and Yeo, K. S.,** 2008: Aerodynamic Forces and Flow Fields of a Two-Dimensional Hovering Wing, *Experiments in Fluids*, Vol. **45**, No. 6, pp. 1047-1065.
- Lian, Y. and Shyy, W.** 2007: Aerodynamics of Low Reynolds Number Plunging Airfoil in Steady and Gusty Environments, *AIAA 2007-79 (Reno)*.
- Miao, J. -M., and Ho, M. -H.,** 2006: Effect of Flexure on Aerodynamic Propulsive Efficiency of Flapping Flexible Airfoil, *Journal of Fluids and Structures*, Vol. **22**, pp. 401-419.
- Milano, M., and Gharib, M.,** 2005: Uncovering the Physics of Flapping Flat Plates with Artificial Evolution, *Journal of Fluid Mechanics*, Vol. **543**, pp. 403-409.
- Muijres, F. T., Johansson, L. C., Barfield, R., Wolf, M., Spedding, G. R., and Hedenström, A.,** 2008: Leading-Edge Vortex Improves Lift in Slow-Flying Bats, *Science*, Vol. **319**, pp. 1250-1253.
- Oo, G. Y., Lua, K. B., Yeo, K. S., and Lim, T. T.,** 2004: Wake Structures of a Heaving Airfoil, *15th Australasian Fluid Mechanics Conference*, Sydney.

- Percin, M.**, 2009: Flow Around a Plunging Airfoil in a Uniform Flow, *MSc. Thesis*, Istanbul Technical University, Istanbul.
- Platzer, M. F., Jones, K. D., Young, J., and Lai, J. C. S.**, 2008: Flapping-Wing Aerodynamics: Progress and Challenges, *AIAA Journal*, Vol. **46**, No. 9.
- Raffel, M., Willert, C., and Kompenhans, J.**, 1998: Particle Image Velocimetry a Practical Guide, Springer Verlag, Berlin.
- Read, D. A., Hover, F. S., and Triantafyllou**, 2003: Forces on Oscillating Foils for Propulsion and Maneuvering, *Journal of Fluids and Structures*, Vol. **17**, pp. 163-183.
- Ringuette, M. J., Milano, M., and Gharib, M.**, 2007: Role of the Tip Vortex in the Force Generation of Low-Aspect-Ratio Normal Flat Plates, *Journal of Fluid Mechanics*, Vol. **581**, pp. 453-468.
- Rival, D., Prangemeier, T., and Tropea, C.**, 2008: The Influence of Airfoil Kinematics on the Formation of Leading-Edge Vortices in bio-Inspired Flight, *Experiments in Fluids*, Vol. **45**, No. 5, pp. 823-833.
- Sarkar, S., and Venkatraman, K.**, 2004: Model Order Reduction of Unsteady Flow Past Oscillating Airfoil Cascades, *Journal of Fluids and Structures*, Vol. **19**, pp. 239-247.
- Schouveiler, L., Hover, F. S., and Triantafyllou, M. S.**, 2005: Performance of Flapping Foil Propulsion, *Journal of Fluids and Structures*, Vol. **20**, pp. 949-959.
- Srigrarom, S., and Vincent, C. W. S.**, 2008: Effect of Pitching and Heaving Motions of SD8020 Hydrofoil on Thrust and Efficiency for Swimming Propulsion, *AIAA 2008-3959 (Seattle)*.
- Sun, M., and Sheikh, S. R.**, 1999: Dynamic Stall Suppression on an Oscillating Airfoil by Steady and Unsteady Tangential Blowing, *Aerospace Science and Technology*, No. 6, pp. 355-366.
- Taylor, G. K., Nudds, R. L., and Thomas, L. R.**, 2003: Flying and Swimming Animals Cruise at a Strouhal Number Tuned for High Power Efficiency, *Nature*, Vol. **95**, pp. 709.
- Theodorsen, T.**, 1935: General Theory of Aerodynamic Instability and the Mechanism of Flutter, *NACA Report 496*.
- Tuncer, I. H., and Platzer, M. F.**, 1996: Thrust Generation due to Airfoil Flapping, *AIAA Journal*, Vol. **34**, No. 2.
- Url-1** <<http://www.dantecdynamics.com>>, date retrieved, 29.10.2011.
- Von Ellenrieder, K. D., Parker, K., and Soria, J.** 2003: Flow Structures Behind a Heaving and Pitching Finite-Span Wing, *Journal of Fluid Mechanics*, Vol. **490**, pp. 129-138.
- Von Ellenrieder, K. D., and Pothos, S.**, 2007: PIV Measurements of the Asymmetric Wake of Two Dimensional Heaving Hydrofoil, *Experiments in Fluids*, Vol. **44**, pp. 733-744.

- Von Karman and Burgers, J. M.**, 1943: General Aerodynamic Theory – Perfect Fluids, *Aerodynamic Theory*, Vol. **2**, pp. 308.
- Van Oudheusden, B. W., Scarano, F., and Casimiri, E. W. F.**, 2006: Non-Intrusive Load Characterization of an Airfoil Using PIV, *Experiments in Fluids*, Vol. **40**, pp. 988-992.
- Wang, Z. J.**, 2000: Vortex Shedding and Frequency Selection in Flapping Flight, *Journal of Fluid Mechanics*, Vol. **410**, pp. 323-341.
- Windte, J., Radespiel, R., Scholz, U., and Eisfeld, B.**, 2004: RANS Simulation of the Transitional Flow Around Airfoils at Low Reynolds Number for Steady and Unsteady Onset Conditions, *NATO RTO-MP-AVT-111*.
- Windte, J., Radespiel, R., and Neef, M.** 2005: Aerodynamic Analysis of Flapping Airfoil Propulsion at Low Reynolds Numbers, *Notes on Numerical Fluid Mechanics and Multidisciplinary Design*, Vol. **89**, pp. 299-313.
- Windte, J., Scholz, U., and Radespiel, R.**, 2006: Validation of the RANS-Simulation of Laminar Separation Bubbles on Airfoils, *Aerospace Science and Technology*, Vol. **10**, pp. 484-494.
- Yadykin, Y., Tenetov, V., and Levin, D.**, 2003: The added mass of a flexible plate oscillating in a fluid, *Journal of Fluids and Structures*, Vol. **17**, pp. 115-123.
- Yang, S., Luo, S., Liu, F. and Tsai, H. –M.**, 2006: Optimization of Unstalled Pitching and Plunging Motion of an Airfoil, *AIAA 2006-1055 (Reno)*.
- Young, J., and Lai, J. C. S.**, 2004: Oscillation Frequency and Amplitude Effects on the Wake of a Plunging Airfoil, *AIAA Journal*, Vol. **42**, No. 10, pp. 2042-2052.
- Young, J.**, 2005: Numerical Simulation of the Unsteady Aerodynamics of Flapping Airfoils, *Phd Thesis*, The University of New South Wales, Sydney.
- Young, J., Lai, J. C. S., Kaya, M. and Tuncer, I. H.**, 2006: Thrust and Efficiency of Propulsion by Oscillating Foils, *3rd International Conference on Computational Fluid Dynamics*, Toronto.
- Young, J., and Lai, J. C. S.**, 2007a: Vortex Lock-In Phenomenon in the Wake of a Plunging Airfoil, *AIAA Journal*, Vol. **45**, No. 2.
- Young, J., and Lai, J. C. S.**, 2007b: Mechanisms Influencing the Efficiency of Oscillating Airfoil Propulsion, *AIAA Journal*, Vol. **45**, No. 7.
- Zhang, H. J., Huang, L., and Zhou, Y.**, 2005: Aerodynamic Loading on a Cylinder Behind an Airfoil, *Experiments in Fluids*, Vol. **38**, pp. 588-593.

APPENDICES

APPENDIX A.1 : List of the Experiments

APPENDIX A.1

Table A.1 : List of the Experiments

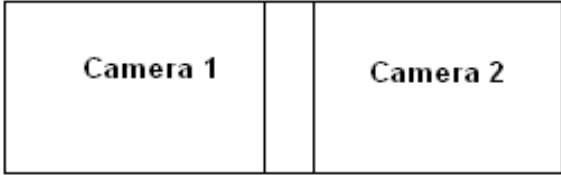
Case	h	f	Re	U (m/s)	d (cm)	α (deg)	k	St	Tail Profile	Camera Position
1	0,25	0,2	5000	0,05	10	0	1,25	0,4	Flat Plate	1
2	0,25	0,2	5000	0,05	5	0	1,25	0,4	Flat Plate	1
3	0,25	0,2	5000	0,05	2,5	0	1,25	0,4	Flat Plate	1
4	0,25	0,2	5000	0,05	Tangent	0	1,25	0,4	Flat Plate	1
5	0,25	0,4	10000	0,1	10	0	1,25	0,4	Flat Plate	1
6	0,25	0,4	10000	0,1	5	0	1,25	0,4	Flat Plate	1
7	0,25	0,4	10000	0,1	2,5	0	1,25	0,4	Flat Plate	1
8	0,25	0,4	10000	0,1	Tangent	0	1,25	0,4	Flat Plate	1
9	0,25	0,4	10000	0,1	10	0	1,25	0,4	NACA 0012	1
10	0,25	0,4	10000	0,1	10	15	1,25	0,4	NACA 0012	1
11	0,25	0,4	10000	0,1	10	30	1,25	0,4	NACA 0012	1
12	0,25	0,4	10000	0,1	5	0	1,25	0,4	NACA 0012	1
13	0,25	0,4	10000	0,1	5	15	1,25	0,4	NACA 0012	1
14	0,25	0,4	10000	0,1	5	30	1,25	0,4	NACA 0012	1
15	0,25	0,4	10000	0,1	2,5	0	1,25	0,4	NACA 0012	1
16	0,25	0,4	10000	0,1	2,5	15	1,25	0,4	NACA 0012	1
17	0,25	0,4	10000	0,1	2,5	30	1,25	0,4	NACA 0012	1
18	0,25	0,4	10000	0,1	Tangent	0	1,25	0,4	NACA 0012	1
19	0,25	0,4	10000	0,1	Tangent	15	1,25	0,4	NACA 0012	1
20	0,25	0,4	10000	0,1	Tangent	30	1,25	0,4	NACA 0012	1
21	0,25	0,4	10000	0,1	Without Tail		1,25	0,4	-	1
22	0,25	0,2	5000	0,05	10	0	1,25	0,4	NACA 0012	1 and 2
23	0,25	0,2	5000	0,05	10	15	1,25	0,4	NACA 0012	1 and 2
24	0,25	0,2	5000	0,05	10	30	1,25	0,4	NACA 0012	1 and 2
25	0,25	0,2	5000	0,05	5	0	1,25	0,4	NACA 0012	1 and 2
26	0,25	0,2	5000	0,05	5	15	1,25	0,4	NACA 0012	1 and 2

Table A.1 (continued): List of the Experiments

Case	h	f	Re	U (m/s)	d (cm)	α (deg)	k	St	Tail Profile	Camera Position
27	0,25	0,2	5000	0,05	5	30	1,25	0,4	NACA 0012	1 and 2
28	0,25	0,2	5000	0,05	2,5	0	1,25	0,4	NACA 0012	1 and 2
29	0,25	0,2	5000	0,05	2,5	15	1,25	0,4	NACA 0012	1 and 2
30	0,25	0,2	5000	0,05	2,5	30	1,25	0,4	NACA 0012	1 and 2
31	0,25	0,2	5000	0,05	Tangent	0	1,25	0,4	NACA 0012	1 and 2
32	0,25	0,2	5000	0,05	Tangent	15	1,25	0,4	NACA 0012	1 and 2
33	0,25	0,2	5000	0,05	Tangent	30	1,25	0,4	NACA 0012	1 and 2
34	0,25	0,2	5000	0,05	Without Tail		1,25	0,4	-	1 and 2
35	0,05	0,4	5000	0,05	10	0	2,5	0,8	NACA 0012	1 and 2
36	0,05	0,4	5000	0,05	10	15	2,5	0,8	NACA 0012	1 and 2
37	0,05	0,4	5000	0,05	10	30	2,5	0,8	NACA 0012	1 and 2
38	0,05	0,4	5000	0,05	5	0	2,5	0,8	NACA 0012	1 and 2
39	0,05	0,4	5000	0,05	5	15	2,5	0,8	NACA 0012	1 and 2
40	0,05	0,4	5000	0,05	5	30	2,5	0,8	NACA 0012	1 and 2
41	0,05	0,4	5000	0,05	2,5	0	2,5	0,8	NACA 0012	1 and 2
42	0,05	0,4	5000	0,05	2,5	15	2,5	0,8	NACA 0012	1 and 2
43	0,05	0,4	5000	0,05	2,5	30	2,5	0,8	NACA 0012	1 and 2
44	0,05	0,4	5000	0,05	Tangent	0	2,5	0,8	NACA 0012	1 and 2
45	0,05	0,4	5000	0,05	Tangent	15	2,5	0,8	NACA 0012	1 and 2
46	0,05	0,4	5000	0,05	Tangent	30	2,5	0,8	NACA 0012	1 and 2
47	0,05	0,4	5000	0,05	Without Tail		2,5	0,8	-	1 and 2

At the Table A.1, camera positions referred with numbers are shown in Table A.2.

Table A.2 : Meaning of the Camera Numbers

Camera Position	Orientation of the Cameras
1	 <p>The diagram shows a horizontal arrangement of two rectangular boxes. The left box is labeled "Camera 1" and the right box is labeled "Camera 2". They are separated by a thin vertical line, indicating they are side-by-side.</p>
2	 <p>The diagram shows a vertical arrangement of two rectangular boxes. The top box is labeled "Camera 1" and the bottom box is labeled "Camera 2". They are separated by a thin horizontal line, indicating they are one above the other.</p>

CURRICULUM VITAE



Name Surname: Ceyhun TOLA

Place and Date of Birth: Ankara – 01.08.1987

E-Mail: ceyhuntola@gmail.com

B.Sc.: 2005 – 2010 Istanbul Technical University, İstanbul, TÜRKİYE
Bachelor of Science, Astronautical Engineering

2007 – 2010 Istanbul Technical University, İstanbul, TÜRKİYE
Bachelor of Science, Aeronautical Engineering
(Double Major)

Professional Experience and Rewards:

- Reward of 1st place in the graduating class of ‘2010 Department of Astronautical Engineering, ITU.
- Reward of graduation from the both Astronautical and Aeronautical Engineering Departments (Double Major) in 4 years at the same time.

List of Publications:

- **Tola, C.**, Aslan, R., Ilarslan, M., 2011: Development of a Mechanical De-orbiting System for a 3Unit CubeSat, 3rd Nano-Satellite Symposium, December 12-13, 2011, Kitakyushu International Conference Center, Japan.
- Aslan, A. R., Oz, I., Gulgonul, S., Sofyali, A., Umit, E., and **Tola, C.**, 2011: TURKSAT-3USAT: A 3U Communication CubeSat with Passive Magnetic Stabilization, 5th International Conference on Recent Advances in Space Technologies RAST 2011, June 09-11, 2011, Harbiye Military Museum and Cultural Center, Turkey.
- Aslan, A. R., Yagci, H. B., Sofyali, A., Suer, M., Umit, E., **Tola, C.**, Ceylan, O., Durna, A. S., Celik, G., and Ozturk, D. C., 2011: Development of a 3Unit CubeSat for LEO Communication, 2nd Nano-Satellite Symposium, March 14-16, 2011, University of Tokyo, Japan.